Agricultural and Forest Meteorology 332 (2023) 109364

Contents lists available at ScienceDirect

Agricultural and Forest Meteorology

journal homepage: www.elsevier.com/locate/agrformet

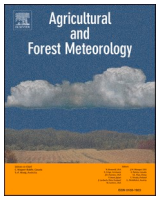

Evaluation and improvement of the E3SM land model for simulating energy and carbon fluxes in an Amazonian peatland

Fenghui Yuan [a,*], Daniel M. Ricciuto [b], Xiaofeng Xu [c], Daniel T. Roman [d], Erik Lilleskov [e], Jeffrey D. Wood [f], Hinsby Cadillo-Quiroz [g], Angela Lafuente [h], Jhon Rengifo [i], Randall Kolka [j], Lizardo Fachin [i], Craig Wayson [d], Kristell Hergoualc'h [k], Rodney A. Chimner [h], Alexander Frie [a,l], Timothy J. Griffis [a,*]

[a] Department of Soil, Water, and Climate, University of Minnesota, Saint Paul, MN, United States
[b] Environmental Sciences Division and Climate Change Sciences Institute, Oak Ridge National Laboratory, Oak Ridge, TN, United States
[c] Biology Department, San Diego State University, San Diego, CA, United States
[d] USDA Forest Service, International Programs, Washington, D.C., United States
[e] USDA Forest Service, Houghton, Michigan, United States
[f] School of Natural Resources, University of Missouri, Columbia, MO, United States
[g] School of Life Sciences and Biodesign Institute, Arizona State University, Tempe, AZ, United States
[h] Michigan Technological University, Houghton, Michigan, United States
[i] Instituto de Investigaciones de la Amazonia Peruana, Iquitos, Peru
[j] USDA Forest Service, Northern Research Station, Grand Rapids, MN, United States
[k] Center for International Forest Research, Lima, Peru
[l] University of Minnesota Sea Grant College Program, Duluth, MN, United States

ARTICLE INFO

Keywords:
Amazon
Peatland
Land surface model
Methane
Tropics
Phenology

ABSTRACT

Tropical peatlands are one of the largest natural sources of atmospheric methane (CH_4) and play a significant role in regional and global carbon budgets. However, large uncertainties persist regarding their feedbacks to climate variations. The Energy Exascale Earth System Model (E3SM) Land Model (ELM) is an ongoing state-of-the-science model, which has developed new representations of soil hydrology and biogeochemistry and includes a new microbial-functional-group-based CH_4 module. This model has been tested in boreal forest peatlands, but has not yet been evaluated for simulating energy and carbon exchange for tropical peatlands. Here, we evaluated the ELM performance in simulating energy, carbon dioxide (CO_2) and CH_4 fluxes of an Amazonian palm swamp peatland in Iquitos, Peru. ELM simulations using default parameter values resulted in poor performance of seasonal carbon dynamics. Several algorithms were improved according to site-specific characteristics and key parameters were optimized using an objective surrogate-assisted Bayesian approach. The modified algorithms included the soil water retention curve, a water coverage scalar function for CH_4 processes, and a seasonally varying leaf carbon-to-nitrogen ratio function. The revised tropics-specific model better simulated the diel and seasonal patterns of energy and carbon fluxes of the palm swamp peatland. Global sensitivity analyses indicated that the strong controls on energy and carbon fluxes were mainly attributed to the parameters associated with vegetation activities, such as plant carbon distribution, stomatal regulation, photosynthetic capacity, and leaf phenology. Parameter relative importance depended on biogeochemical processes and shifted significantly between wet and dry seasons. This modeling study advanced the understanding of biotic controls on the energy and carbon exchange in Amazonian palm swamp peatlands and identified knowledge gaps that need to be addressed for better prediction of carbon cycle processes and budgets for tropical peatlands.

* Corresponding authors.
E-mail addresses: fyuan@umn.edu (F. Yuan), tgriffis@umn.edu (T.J. Griffis).

https://doi.org/10.1016/j.agrformet.2023.109364
Received 14 May 2022; Received in revised form 6 January 2023; Accepted 7 February 2023

1. Introduction

Natural tropical peatlands are an important global carbon sink accumulating large amounts of carbon in soils over centuries. Concurrently, they are also large methane (CH_4) sources. Based on tropical peatland distribution (Gumbricht et al., 2017) and a multi-model estimate of peatland emissions (Melton et al., 2013), tropical peatlands could account for about 25% of global peatland CH_4 emissions, however, these emissions are poorly constrained. According to recent global peatland distribution estimates, the largest areas of tropical peatlands are found in South America and Southeast Asia (Gumbricht et al., 2017). The peatlands of South America account for approximately 44% of tropical peatlands by area and volume (Gumbricht et al., 2017). In Southeast Asia, the carbon dynamics of tropical peatlands have been well studied over the past decades and this region has generally been identified as a major carbon source to the atmosphere as a result of land-use change and fires (Lilleskov et al., 2019; Ribeiro et al., 2021). In contrast, observations from tropical peatlands in South America remain scarce. For example, according to current global and regional carbon observation databases, such as FLUXNET, AmeriFlux, ICOS, AsiaFlux, OzFlux and ChinaFlux, as of April 18, 2022, less than 10% of global eddy covariance (EC) sites are in the tropics, and only one of these sites (this study) represents Amazonian peatlands. Consequently, we have a poor understanding of how these ecosystems function and respond to climate variability leading to large uncertainties about their carbon cycle processes and budgets (Griffis et al., 2020). Indeed, several studies indicate that the differences between bottom-up and top-down estimates of CH_4 and carbon dioxide (CO_2) budgets range from 40% to 700% in tropical South America (Meng et al., 2015; Ribeiro et al., 2021; Zhang et al., 2017).

Comprehending and predicting carbon cycle processes in terrestrial ecosystems and their responses to environmental changes requires integrating empirical research and field observations with modeling efforts that include mathematical and computational representations. Model simulation of carbon cycle processes for peatlands is complex and relies on the coupling among many specific biophysical and biogeochemical submodels, e.g., energy transport, hydrological, soil carbon mineralization, and canopy photosynthesis. Several studies have used different land surface models (LSMs) to estimate the CH_4 emissions and CO_2 fluxes from wetlands at regional and global scales (e.g., Largeron et al., 2018; Melton et al., 2013; Paudel et al., 2016; Riley et al., 2011; Zhang et al., 2017; Zhuang et al., 2006). At the site scale, LSMs have been widely applied to temperate and boreal peatlands (e.g., Ma et al., 2021; Ricciuto et al., 2021; Yuan et al., 2021a, 2021b); however, despite the importance of tropical peatlands, few modeling studies have reported their carbon flux simulations (Farmer et al., 2011; Kurnianto et al., 2015), mainly due to the scarcity of tropical peatland observations for model parameterization and evaluation. In addition, tropics-specific model development has faced many challenges in achieving high performance ecosystem carbon cycle simulations. For example, recent studies recognized that most LSMs are unable to capture seasonal variations in canopy photosynthesis and transpiration of Amazonian evergreen forests (Chen et al., 2020), because traditional plant-functional-type (i.e., tropical broadleaf evergreen trees) parameters are not able to adequately represent the leaf phenology of these complex ecosystems where a dry season increase in canopy gross primary production (GPP) is linked to new maturing leaves (Saleska et al., 2016; Wu et al., 2016, 2020).

Another critical challenge for the peatland model simulation is how to mechanistically represent the carbon-related microbial processes. It is well recognized that microbial activities fundamentally drive peatland carbon dynamics in soils (Bridgham et al., 2013; Dean et al., 2018; Xu et al., 2016). For example, microbe-mediated soil organic matter mineralization provides dissolved organic carbon as the available carbon for CO_2 and CH_4 production. Acetoclastic and hydrogenotrophic methanogenesis dominate most biological CH_4 production from acetate, CO_2 and H_2. Microbial oxidation of CH_4 is controlled mainly by aerobic and anaerobic methanotrophy. In addition to substrate quantity and quality, and oxygen availability, methanogenesis and methanotrophy are also directly and indirectly controlled by soil pH, temperature, moisture, and abundance of different terminal electron acceptors (TEA) (Bridgham et al., 2013; Dean et al., 2018; Riley et al., 2011; Xu et al., 2016). Because of limited measurements and the complexity of biogeochemical processes in peatlands, most LSMs do not explicitly represent microbes and their controls on carbon cycling.

Our team recently established an EC flux site in a protected natural Amazonian palm swamp peatland near Iquitos, Peru (Griffis et al., 2020). Measurements from the site are helping to improve our understanding of tropical peatland biogeochemical processes. We have reported the ecosystem-scale observational CO_2 and CH_4 fluxes and budgets for this Amazonian palm swamp peatland (Griffis et al., 2020). These data suggest that the peatland is acting as a significant long-term and year-round carbon sink (e.g., −253 to −627 gC m^{-2} y^{-1} in 2019). We have also implemented a new wetland version for the land component of the Energy Exascale Earth System Model (ELM) to increase our capacity to diagnose and forecast changes in the carbon balance of these tropical peatland ecosystems (Ricciuto et al., 2021). ELM has recently added several key microbial mechanisms and processes, such as methanogenesis based on H_2 and CO_2 (hydrogenotrophic methanogenesis), methanogenesis based on acetate (acetoclastic methanogenesis), aerobic methanotrophy, anaerobic methanotrophy, and H_2 production, which have improved the simulations of carbon cycle processes in temperate and boreal peatlands (Ricciuto et al., 2021; Xu et al., 2015). This model has been comprehensively evaluated and successfully applied to a boreal peatland (Shi et al., 2021; Yuan et al., 2021a, 2021b), but has not been applied to tropical peatlands.

The objectives of this work, therefore, were to: 1) Evaluate the performance of ELM in simulating the energy and carbon fluxes for the Amazonian palm swamp peatland; 2) Diagnose and improve model deficiencies and biases; and 3) Identify the key parameters and associated processes controlling the variability of energy and carbon fluxes. First, we tested the ability of ELM with default parameters and modified several key parameter algorithms according to site-specific characteristics. Second, based on the improved model, a Monte Carlo parameter sensitivity analysis and optimization was conducted using a surrogate-assisted machine learning approach. Finally, the diel and seasonal simulations for energy and carbon fluxes were evaluated against EC observations over the period 2018 - 2019.

2. Methodology

2.1. Study site and observations

This study was conducted at the AmeriFlux site PE-QFR (3°50′03.9″ S; 73°19′08.1″ W), a protected natural palm swamp peatland forest located near Iquitos in the Loreto region in the Peruvian Amazon. The dominant tree species are *Mauritia flexuosa* palms (61%) and *Tabebuia insignis* (15%) (Mitidieri, 2014). The current vegetation community was established ca. 400 years ago (Roucoux et al., 2013). *M. flexuosa*-dominated palm swamp forests are the dominant peatland type in the Peruvian Amazon (78%). The average canopy height at this site is 21.3 m and mean annual leaf area index (LAI) estimated from satellite observations ranged from 3.9 to 4.9 m^2 m^{-2} in 2018 and 2019, respectively (Griffis et al., 2020). The lower canopy layer was dominated by dicot individuals (such as *T. insignis*), while the upper canopy was dominated by palms. The peat thickness varies from 1.9 to 2.5 m (Bhomia et al., 2019) with a total soil C pool of ~740 Mg C ha^{-1}. The site is characterized by a tropical wet-dry climate. Mean annual air temperature and precipitation from 2003 to 2017 were 27.2 °C and 2753.2 mm, respectively. The “wet” high-rain season is typically from February to April with mean air temperature at 27.4 °C and accumulated precipitation of 810 mm; the “dry” low-rain season is typically from

August to September with mean air temperature at 27.6 °C and precipitation of 545 mm (Griffis et al., 2020). If microtopographic heterogeneity is not considered, this site is quasi-permanently waterlogged with > 10 cm water table (Hergoualc'h et al., 2020) and a terrain slope that is generally less than 2%.

Meteorological and micrometeorological instruments were installed at this site in 2017. Variables measured or calculated include half-hour EC fluxes of energy, water vapor, CO_2 and CH_4, air temperature, relative humidity, precipitation, global solar radiation, net radiation (R_n), and photosynthetically active radiation (PAR) at a height of 40 m. We did not force energy balance closure of the EC flux measurements prior to model comparisons. Ancillary measurements include soil volumetric water content and soil heat flux at 10 cm depth, and water table level is recorded in a shallow well. Note that the CH_4 observations were unavailable in 2018 due to lightning strike instrument damage. More details on the site, instruments and flux data processing have been reported by Griffis et al. (2020).

2.2. Model description and simulation procedures

ELM, the land component of E3SM, is based upon the Community Land Model (CLM4.5, Oleson et al., (2013). A peatland version of ELM, ELM-SPRUCE, includes improved representation of microtopography and hydrology (Shi et al., 2015), a new plant functional type of *Sphagnum* moss (Shi et al., 2021), and new microbial functional group-based CH_4 cycling (Ricciuto et al., 2021; Xu et al., 2015). ELM-SPRUCE, originally designed to simulate a northern Minnesota bog, is further developed here for tropical peatland simulations.

The implementation of the model simulations included three phases. The first two phases, accelerated decomposition (AD) spin-up and final spin-up, follow the same strategy used for CLM4.5 (Thornton and Rosenbloom, 2005). The AD-spin-up simulation of 600 years allowed the system to accumulate carbon and reach an equilibrium state in an accelerated mode. A 50-year final spin-up subsequently allowed the system to operate with normal decomposition parameters before conducting transient (contemporary) simulations. The third phase included transient simulations running from 1980 to 2020. Following model function improvements and parameter optimization, all three phases were repeated. The model results for 2018 and 2019 in the third phase were used to evaluate the model performance in this study.

The hourly atmospheric forcing data (from 2018 to 2019) were obtained from the PE-QFR site, including air temperature, specific humidity, solar radiation, wind speed, air pressure, PAR and precipitation. Due to missing values (< 20%) in the observed precipitation, hourly ERA5 (https://doi.org/10.24381/cds.adbb2d47) reanalysis precipitation was used to fill these gaps. For all three model simulation phases, we repeatedly cycled the 2-year forcing data as offline runs. Morphological and physiological parameters of a single plant functional type (tropical broadleaf evergreen tree) was used to define the tree species at this site. Default values for vegetation, soil and microbial parameters in ELM-SPRUCE were used for the initial model simulations (Table S1).

2.3. Model improvement

Initial simulations using ELM-SPRUCE with default parameters resulted in poor representation of the carbon dynamics for this Amazonian palm swamp peatland, mainly because the annual seasonality and dynamics in CO_2 and CH_4 fluxes were not well simulated (Fig. S1). To improve the seasonal performances, parameter optimization was conducted for the default model as described in Section 2.4. However, the final 'optimal' parameter values for the default model were still not able to yield realistic simulations, indicating the model-observation difference cannot be resolved through model parameter optimization alone. We further found that the poor simulations were primarily related to unrealistic descriptions of peat soil water retention, hydrological controls on CH_4 processes, and seasonal behavior of canopy assimilation for this peatland in the default model. The three corresponding model algorithms of ELM-SPRUCE were then modified according to site-specific characteristics with subsequent parameter optimization. Detailed procedures are presented in the Supplementary Material, and a summary of the modifications is presented here:

Soil water retention curve. According to the field measurements by Iiyama et al. (2012), we replaced the default soil water retention function with the van Genuchten function (van Genuchten, 1980) as Equation 1 in Section 1.1 of the Supplementary Material. The new function can produce higher residual water content, which is more realistic for tropical peat than the Clapp and Hornberger function in the default model (Fig. S2).

Water coverage scalar for CH_4 *processes*. We included a simple water coverage scalar ($f_{inundation}$) for the Amazonian palm swamp peatland in the model (Section 1.2 in the Supplementary Material, Fig. S3). Acetate production and CH_4 production, oxidation, and transport are limited by this scalar when the ground surface is not fully covered by water. The scalar is calculated using a water table level dependence based on the observational relationship of water table level (below ground surface) and ecosystem CH_4 fluxes (Griffis et al., 2020).

Seasonally varying leaf carbon-to-nitrogen ratio. Although ELM-SPRUCE assumes a constant leaf carbon-to-nitrogen ratio (C/N ratio), we hypothesized that there is seasonality in this C/N ratio in this Amazonian palm swamp peatland following the same temporal trend as other Amazonian forests. According to field measurements from other studies (Carswell et al., 2000; Chavana-Bryant et al., 2017; Parolin et al., 2002), we developed an empirical bell-shaped function describing the leaf C/N ratio change with aging as given in Equation 3 of Section 1.2 in the Supplementary Material (Fig. S4). The function was integrated into the Farquhar-von Caemmerer-Berry (FvCB) submodel for canopy photosynthesis within ELM.

2.4. Parameter sensitivity and optimization

To identify the key parameters controlling the variability of energy and carbon fluxes and to reduce the discrepancies between model simulations and observations, model parameter sensitivity and optimization were conducted with the Markov Chain Monte Carlo (MCMC) approach and a neural-network-based surrogate model. These procedures were performed using a novel tool — the Offline Land Model Testbed (OLMT) (Ricciuto et al., 2018). The OLMT performs model ensembles using different parameter combinations and provides post-processed model outputs to the Uncertainty Qualification Toolkit (UQTk) (Ghanem et al., 2016) to analyze parameter sensitivities. OLMT also builds surrogate models for selected model outputs that can be used for parameter optimization with reduced computational cost. More detailed information about the methods and tools can be found in the studies by Safta et al. (2015) and Ricciuto et al. (2018). Briefly, there were three key steps for the parameter sensitivity and optimization procedure:

1) *Initial sampling*. 65 key parameters that play a role either directly or indirectly in carbon dynamics were initially selected for parameterization (Table S1). These adjustable parameters are relevant to surface energy exchange, hydrology, soil biogeochemistry, and plant physiology. The ranges of these parameters were obtained from published papers to constrain parameter sensitivity and optimization (Ricciuto et al., 2018; Xu et al., 2015). After their prior uniform distributions were defined, 6000 parameter sets were randomly sampled within their acceptable ranges using a Monte Carlo sampling technique.
2) *Global sensitivity analysis.* First-order Sobol index (also known as the main effect) and total Sobol index (also known as the joint total effect) were used to quantify the parameter sensitivity using a Bayesian compressive sensing method with UQTk (Sargsyan et al., 2014). Because the main effect index measures the fractional contribution of the total variance resulting from an independent parameter and all

interactions with other parameters, it can also help diagnose each parameter's total role in determining specific output variation. The joint total effect includes the sensitivity of both first order effects as well as the sensitivity due to interactions between a given parameter and all other parameters, and it is used to identify the parameter interactions. In this study, CO_2 fluxes, CH_4 fluxes, gross primary production (GPP), ecosystem respiration (ER), and latent heat fluxes (LE) were selected as output quantities of interest (QoI). To identify the seasonal patterns of parameter sensitivities, specific wet and dry seasons were distinguished for each QoI according to Griffis et al., (2020) (wet season is DOY 32–120 in both 2018 and 2019; dry season is DOY 152–304 in 2018 and DOY 213–273 in 2019, respectively). After ranking the sensitivity indices of all parameters in the OLMT, the 21 most sensitive parameters were identified for each output of interest in different seasons (see Section 3.1).

3) *Parameter downselection and optimization.* For the most sensitive parameters above, the 21 - dimensional parameter set was then again randomly sampled from their prior ranges; the other 44 less-sensitive parameters were omitted given their non-significant impacts on the model outputs (QoIs). Next, using the OLMT, we performed a second model ensemble with 4000 ELM simulations, and conducted a second sensitivity analysis with UQTk on these 21 parameters. We constructed neural network-based surrogate models for each of the corresponding model outputs matching these observations, using the 4000 ensemble simulations for training and validation. When building the surrogate models, 80% of the ensemble members were randomly selected for training and the remaining 20% were retained for independent cross-validation. MCMC was then used to optimize the 21 model parameters using 100,000 evaluations for each surrogate model and the corresponding observations (Safta et al., 2015).

2.5. Model evaluation

Hourly outputs from ELM were used for examining the diel cycles of LE, sensible heat fluxes (H), GPP, ER, net ecosystem exchanges of CO_2 and CH_4. Daily outputs were used for examining their seasonal patterns. Since we only have the observational data of CH_4 fluxes in 2019, we took the 2019 data as an example for representing the diel behavior in this study. Taylor diagrams were used to represent the statistical comparisons of seasonal model performances against observations with three statistical tests, including Pearson correlation coefficient (r), root mean square error (RMSE), and the standard deviation (SD) ratio between the simulated and observed results.

3. Results and discussion

3.1. Parameter optimization

Compared to default values in ELM, the values of 21 key parameters were changed after optimization with the Bayesian inference analysis (Table 1). These parameters mainly related to photosynthesis, phenology and CH_4 production and transport. Specifically, both parameters of the base rate of plant maintenance respiration (*br_mr*) and its temperature sensitivity (*q10_mr*) decreased compared to the default values for tropical broadleaf evergreen trees in ELM, indicating less maintenance respiration costs during plant growth and lower temperature dependence of maintenance respiration. The carbon allocation parameters were optimized with lower fraction of nitrogen allocated to RuBisCO enzyme (*flnr)* and higher fine root to leaf allocation ratio (*froot_leaf)*. The optimized *flnr* (0.1135) was very close to the value reported for oil palm (0.1005, Fan et al., 2015). A higher optimized Ball–Berry stomatal conductance slope (*mp*, 7.0) indicates higher stomatal conductance and lower stomatal efficiency, which was well within the range of seasonally dry Amazonian forests (5.98 - 8.85, average 7.38, Wu et al., 2020). Compared with the default values, the parameters of vegetation phenology (*leaf_long*) and canopy leaf area distribution (*slatop*) also increased. Optimized *leaf_long* and *slatop* were also consistent with previous studies for the oil palm (Fan et al., 2015). For the microbial controls on CH_4 fluxes, acetoclastic methanogenesis parameters (*m_dAceProdACmax* and *m_dYAceMethanogens*) were reduced, however, the decomposition rate of dissolved organic matter (*k_dom*) and plant-mediated CH_4 transport (*m_dPlantTrans*) were enhanced after parameter optimization. Although direct evaluation of these CH_4-related parameter values could not be conducted in this study, previous observations from other Amazonian peatlands can provide some insights. For example, the contribution of acetoclastic methanogenesis to CH_4 production was found to be lower (Finn et al., 2020; Holmes et al., 2015), and the contribution of plant transport to total CH_4 fluxes was higher (van Haren et al., 2021) compared to temperate and boreal peatlands (see Section 3. 4 and 3.5), implicitly supporting these optimization results.

Well-defined parameter bounds can provide a strong constraint for

Table 1
Default values and bound constraints of 21 key parameters and their final optimized values against observations. Most information on parameter bounds was from the summaries by Ricciuto et al. (2018) and Xu et al. (2015). For the parameters not included in their papers (*), their bounds were defined as +/- 50% of the default values in the ELM-SPRUCE version. ** means the average of all plant functional types in the default model.

Parameter	Initial range	Default value	Optimized value	Description
bdnr	0.125–0.375	0.141	0.141	Bulk denitrification rate
br_mr	1.26e-6 - 3.75e-6	3.75E-06	1.50E-06	Base rate for maintenance respiration (gC gN^{-1} s^{-1})
dleaf	0.01 - 1	0.04	0.04	Characteristic leaf dimension
fcur	0 - 1	1	1	Fraction of allocation that goes to current growth
flnr	0.0231 - 0.264	0.2014**	0.1135	Fraction of leaf N in RuBisco
froot_leaf	0.3 - 2.5	0.5645**	2.5	Fine root to leaf allocation ratio
frootcn	21 - 63	45.25**	42	Fine root C:N ratio
leaf_long	0 - 7	1.1**	1.78	Leaf longevity (years)
livewdcn	25 - 75	0.763	0.763	Live wood C:N ratio
mp	4.5 - 13.5	4.23	7.0	Ball-Berry slope parameter
q10_mr	1.3 - 3.3	2.21	1.3	Temperature sensitivity for plant maintenance respiration
r_mort	0.0025 - 0.05	0.05	0.05	Mortality rate
slatop	0.002 - 0.03	0.009*	0.012	Specific Leaf Area (SLA) at top of canopy
k_dom	0.00595–0.0375	0.007	0.025	Decomposition rate of dissolved organic matter
m_dAceProdACmax	1e-08 - 0.035	2.40E-06	1.00E-07	Maximum rate of acetic acid production from available carbon (mmol m^{-3} h^{-1})
m_dACMinQ10	1.5 −4.5*	3	3	Temperature sensitivity of available carbon mineralization
m_dGrowRAceMethanogens	0.004 - 2.88	0.008	0.008	Growth rate of acetoclastic methanogens (day $^{-1}$)
m_dH2ProdAcemax	2.5e-09 - 1.24	5.00E-08	5.00E-08	Maximum reaction rate of conversion of H_2 and CO_2 to acetic acid (mmol acetate g^{-1} h^{-1})
m_dYAceMethanogens	0.037–0.3	0.2	0.162	Growth efficiency of acetoclastic methanogens (mol C mol acetate C^{-1})
m_dKCH4OxidCH4	0.0025 - 1.5*	1	1	Half-saturation coefficient of CH_4 oxidation for CH_4 concentration (mmol L^{-1})
m_dPlantTrans	0.008–17.2	0.00595	0.014	Parameter for plant-mediated transport

the parameter optimization and reduce parametric uncertainties. Several optimized parameters were very close to their defined bounds after optimization, i.e., *froot_leaf* and *r_mort* (vegetation mortality rate) met their upper bounds, while *q10_mr* hit its lower bound. A possible reason is that the optimization attempted to compensate for structural discrepancies between model simulations and observations by pushing these parameters toward either the minimum or the maximum of their given bounds (Ricciuto et al., 2018). This might imply that these optimized values can be further improved by extending the defined parameter bounds. Additional field investigations need to be conducted to assess the reasonableness of current vs. expanded bounds.

The improvement and optimization procedures greatly enhanced the magnitude and seasonality of the simulated energy and carbon fluxes for the Amazonian palm swamp peatland. Fig. 1 shows the different model performances for LE, GPP, ER, CO_2 fluxes, and CH_4 fluxes with optimized and default parameter values against the observation data. In the default simulations, we did not find pronounced seasonal patterns of energy and carbon exchanges. In contrast, the improved model yielded marked improvements in GPP, CO_2 fluxes, and CH_4 flux simulations that matched the observations much better than the default model, especially the dramatic change between dry and wet seasons (Fig. 1b, c, e). This resulted mainly from the difference between optimized and default functions (hydrological and C/N ratio functions) and parameters (e.g., *leaf_long, slatop, flnr*, and *froot_leaf*), which are closely related to the representations of seasonal hydrological conditions and phenology of photosynthesis. The improvements for LE and ER simulations were relatively small, although their simulated values were still within or overlapped observation uncertainty ranges as measured by the 95% confidence intervals (Fig. 1a, d). Relatively poor performance on the seasonality of LE and ER indicates that their response to the changing

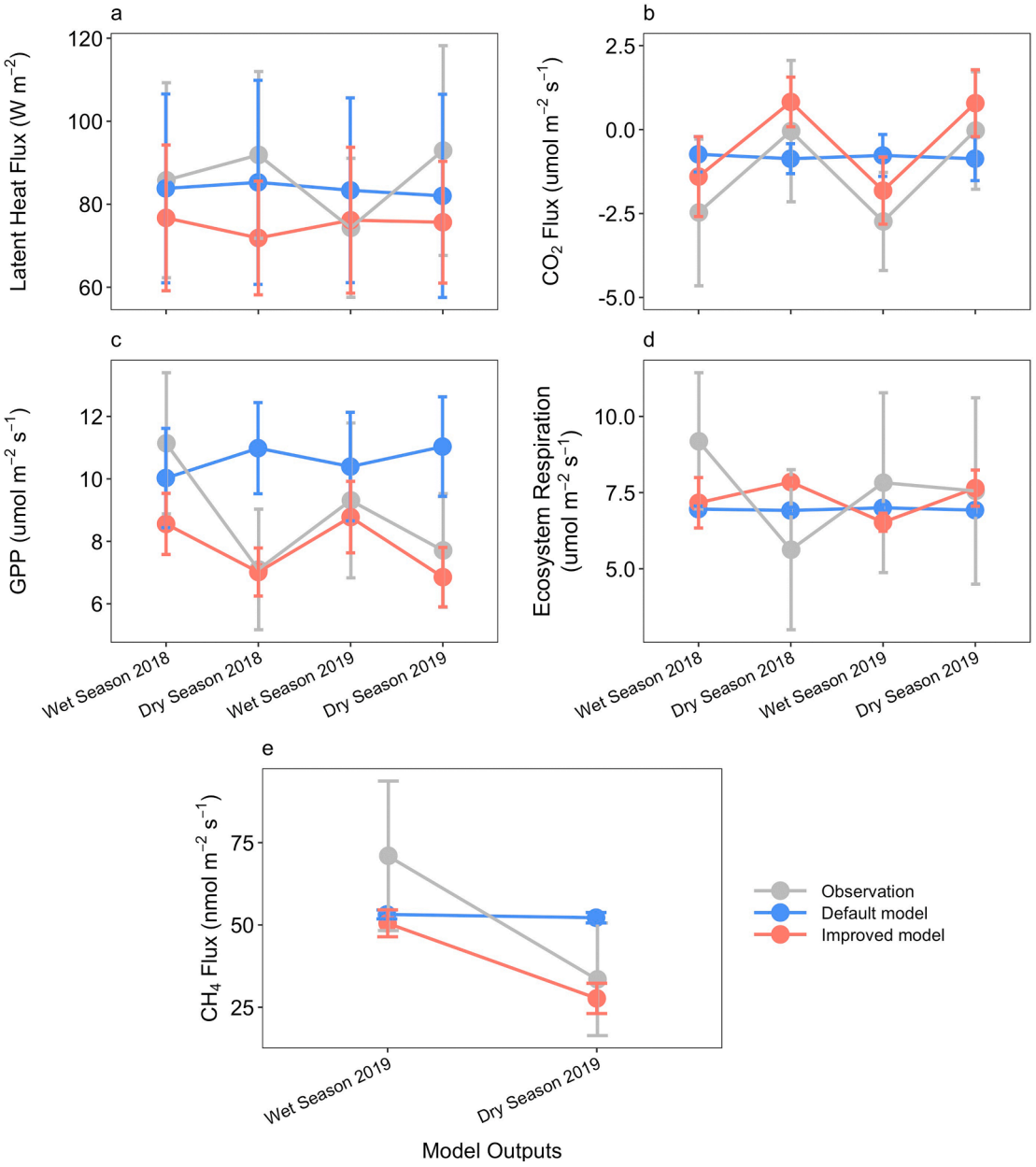

Fig. 1. Seasonal differences between simulated and observed variables caused by parametric uncertainty. Variables are latent heat fluxes (LE), gross primary production (GPP), ecosystem respiration (ER), CO_2 fluxes, and CH_4 fluxes. All data are the average values corresponding to wet and dry seasons in 2018 and 2019. Red represents the simulation with optimized parameter set with 95% confidence interval. Blue represents the simulation with default parameters with 95% confidence interval. Gray indicates observational variable with standard deviation.

environment conditions was not captured very well within the annual time scale. These model-observation differences might be caused by unidentified model structural errors as well as model parameter errors (see Sections 3.2 and 3.3). The improved model clearly reduced the parametric uncertainty bounds for GPP and LE compared to the default model, and increased the uncertainty bounds for ER, CO_2 and CH_4 fluxes. The parametric uncertainties varied according to different output variables, probably due to the impacts from other potential influencing processes or parameters related to the energy and carbon fluxes in the Amazonian palm swamp peatland (see Sections 3.2 and 3.3). With magnitudes and uncertainty bounds of the CO_2 fluxes differing between optimized and default simulations, the PE-QFR site represented different carbon sink/source functions. For example, the simulation using the default parameters indicated the site always acted as a net carbon sink, while the optimized simulation indicates that the site was a net carbon source during the dry seasons (Fig. 1b). However, both simulations were

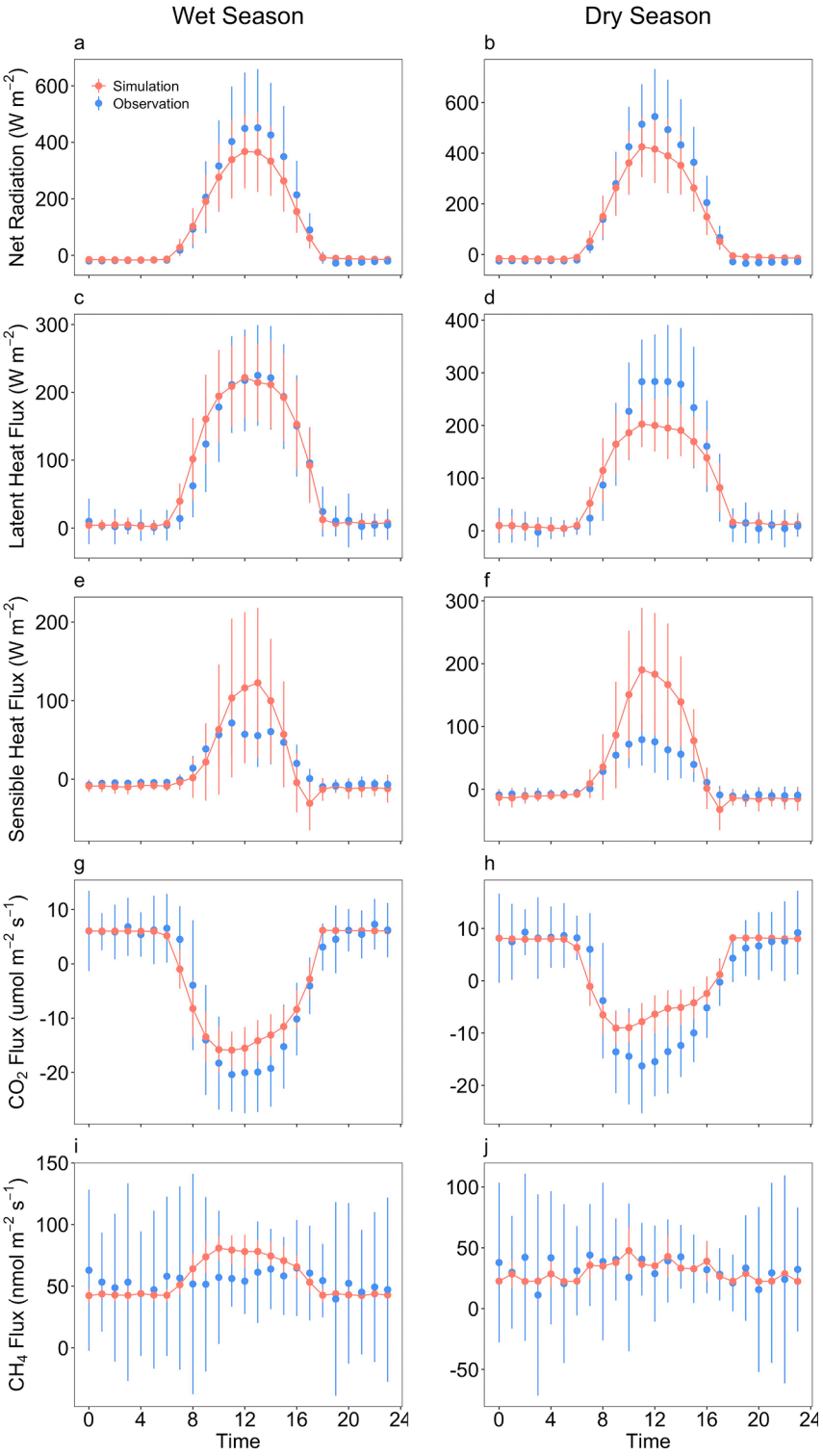

Fig. 2. Comparing diel patterns (mean ± standard deviation) of simulated and observed hourly net radiation (R_n), latent heat fluxes (LE), sensible heat fluxes (H), CO_2 fluxes, and CH_4 fluxes for wet and dry seasons in 2019.

all enclosed within the large observation uncertainty bounds of the CO_2 fluxes. The fact that the upper observation uncertainty bounds were also above zero during dry seasons further indicates that the optimized simulation had nearly consistent estimation for the CO_2 fluxes.

3.2. Net radiation and turbulent energy exchange

The improved ELM model simulated diel patterns of R_n and turbulent energy fluxes (LE and H) that were in relatively good agreement with the observations (Fig. 2a - f). Taking the 2019 wet season as an example, the simulated diel pattern for LE was in excellent agreement with the observations with peak midday values of 220.4 W m^{-2} (225.1 W m^{-2} for observations). However, the simulated maximum for R_n was underestimated by about 83.9 W m^{-2} and the simulated peak of H was 72% higher than the observations. For the 2019 dry season, ELM underestimated R_n and LE from 10:00 to 15:00. It simulated lower than observational R_n peak by 22%, and lower than observational LE peak by 28%. In contrast, ELM overestimated H from 11:00 to 14:00 in the 2019 dry season, with a simulated midday peak of 191.6 W. m^{-2} (79.2 W m^{-2} for observation peak).

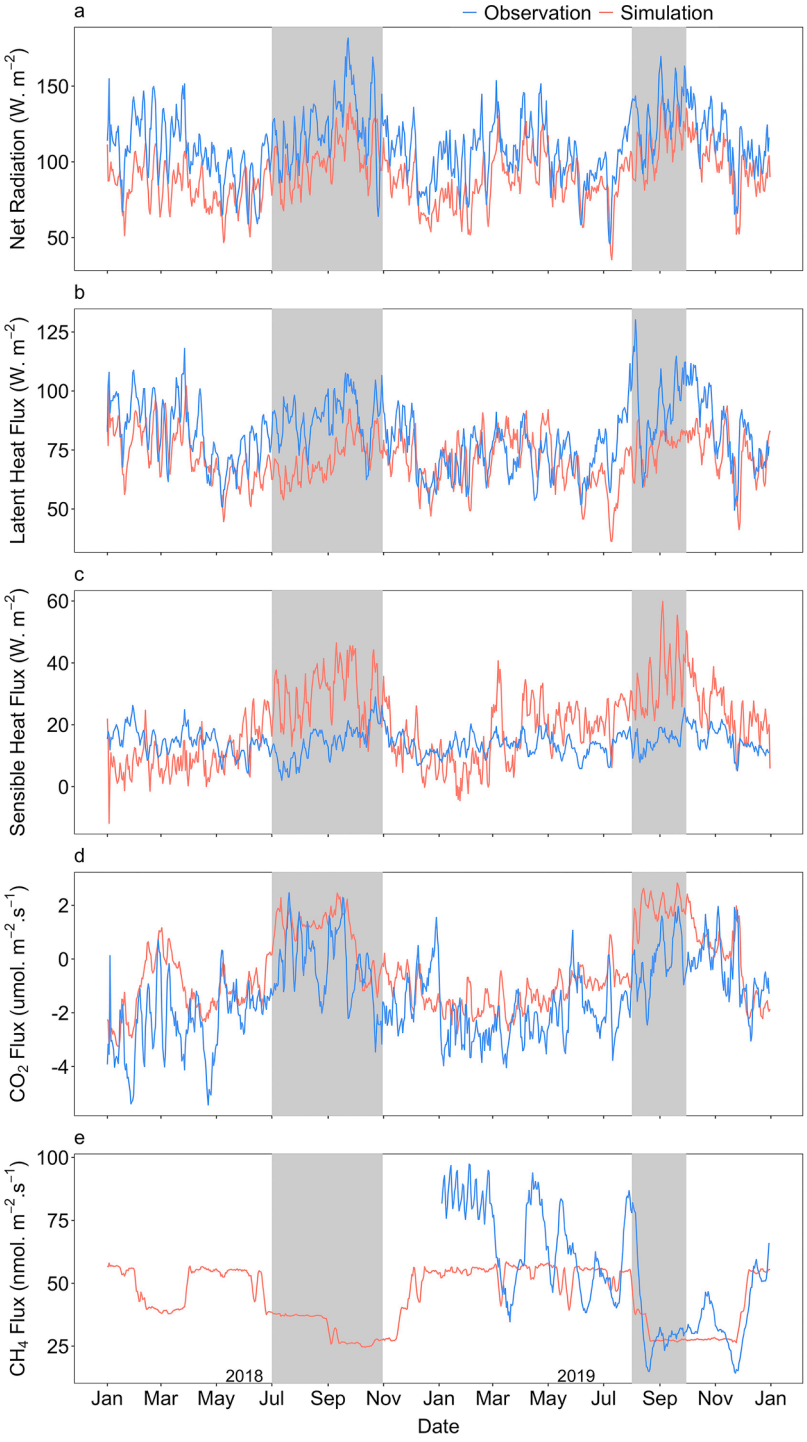

Fig. 3. Comparing seasonal patterns of simulated and observed daily average (5-day moving average) net radiation (R_n, a), latent heat fluxes (LE, b), sensible heat fluxes (H, c), CO_2 fluxes (d) and CH_4 fluxes (e) in 2018 and 2019. (Shade shows dry seasons according to Griffis et al., 2020).

ELM simulated the seasonal patterns of daily R_n and energy fluxes reasonably well with maximum values occurring during the dry seasons and minimum values during the wet seasons (Fig. 3a - c). The model performance of seasonal R_n and LE were generally better than for H when compared to the observations. However, there were important inconsistencies in the range of simulations and observations. Fig. 3a - c indicate the underestimations for R_n and LE and overestimation for H existed during the dry seasons, which is comparable with the disagreements of their diel patterns. For example, in 2019 the annual peak of the simulated LE was 113.6 W m^{-2} and its minimum was 11.1 W m^{-2}, 31.8% and 24.0% lower than the observations, respectively. The simulated H peaked at 72.3 W m^{-2} and reached a minimum value of −28.1 W m^{-2}, while the observations revealed lower single observed maximum and minimum H of 35.3 W m^{-2} and −3.2 W m^{-2}, respectively.

The Taylor diagrams in Fig. 4a - c also show better performances for R_n and LE compared to H. The simulated R_n in both years had high correlation with the observations (r = 0.91), similar SD (13.5 W m^{-2}), and low RMSE (20.4 W m^{-2}). The model performance of R_n was similar between the two years. For LE, the simulations showed higher correlation with the observations in 2018 (r = 0.75) compared to 2019 (r = 0.44). However, the differences in RMSE and SD between the two years were not large, with averaged RMSE = 13.0 W m^{-2}, and averaged SD =7.4 W m^{-2}. This indicates that the model performance for R_n and LE was relatively stable between years. In contrast, the simulated H showed more pronounced variability in performance. Compared to 2018 (RMSE = 11.3 W m^{-2}, r = 0.02, and SD =10.6 W m^{-2}), the simulations of H in 2019 performed better with higher r (0.69) and lower SD (9.5 W m^{-2}) and a larger RMSE (11.5 W m^{-2}). The model's ability to simulate H of tropical peatlands is to some extent linked to distinct hydrological conditions between years. For example, the precipitation rate in wet/dry seasons of 2018 and 2019 were 8.7/5.8 mm d^{-1} and 11.0 /4.9 mm d^{-1}, respectively.

We hypothesize that the discrepancies were caused by model bias in transpiration, LAI, and turbulence exchange associated with the single-layer canopy scheme (i.e., the 'big leaf' assumption) in ELM. First, the deficiencies in simulating canopy transpiration may be a key cause of the model vs observation bias in LE. At this study site, the soil water is always near or well above field capacity with a water table near the surface. The air temperature is relatively stable and high during the wet and dry seasons. For example, the mean air temperatures were 26.0/26.1 °C and 25.6/26.2 °C for the 2018 and 2019 wet/dry seasons, respectively (Griffis et al., 2020). Transpiration is expected to dominate evapotranspiration given the relatively high canopy LAI. The simulations indicate that the transpiration accounted for 45.2 – 53.8% of evapotranspiration during the wet seasons and 63.8 – 65.7% in the dry seasons (Fig. S5). This implies that a bias in transpiration can significantly influence the relative partitioning of the turbulent heat fluxes that would be more pronounced during the dry seasons. The diel simulations further indicated that underestimated daytime LE occurred mainly in the dry seasons (Fig. 2d). In contrast, evidence suggests that during the dry seasons the higher VPD causes downregulation of canopy photosynthesis; however, no significant impact of VPD on LE was found because of enough soil water supply (Griffis et al., 2020). A number of Amazonian forest studies have shown that, LE is strongly controlled by R_n rather than soil water availability as predicted by LSMs (Griffis et al., 2020; Restrepo-Coupe et al., 2021). In addition, some studies suggested that the static process – based stomatal conductance model, such as Ball-Berry model used in ELM, cannot capture the trade-off between hydraulic and stomatal regulation (Oliveira et al., 2021), especially for

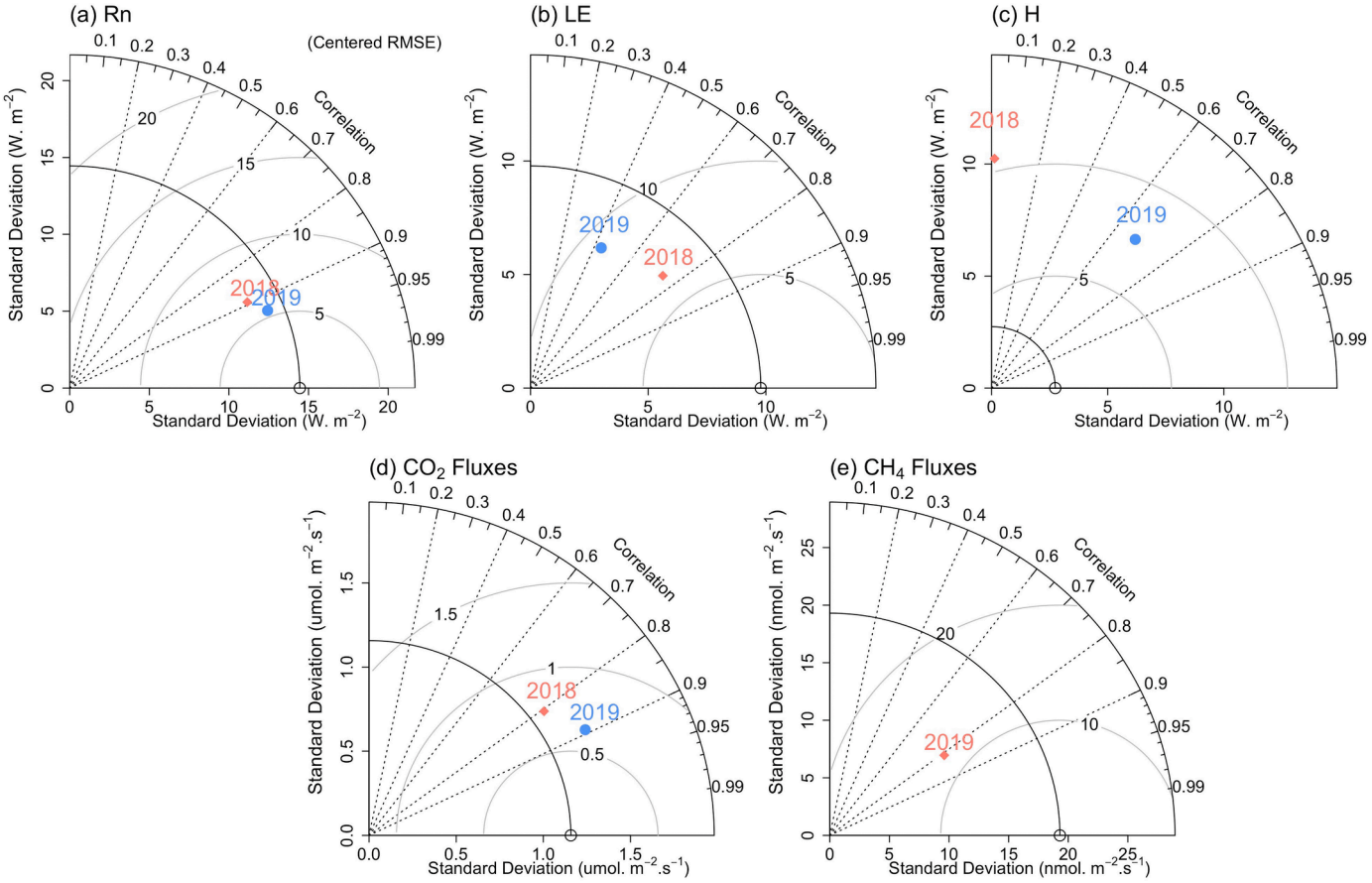

Fig. 4. Taylor diagrams showing correlations coefficients (dotted contours), standard deviations (black solid contours) and RMSEs (gray solid contours) between daily observations (net radiation R_n, a; latent heat fluxes LE, b; sensible heat fluxes H, c; CO_2 fluxes, d; and CH_4 fluxes, e.) and ELM simulations in 2018 and 2019.

the potential atmospheric dryness during the dry seasons. Other studies that applied LSMs over the Amazon region also reported an underestimation of evapotranspiration (Baker et al., 2021; Werth and Avissar, 2004). These studies provide additional evidence for the modeling biases related to vegetation control and the downregulation of stomatal conductance during the dry season (Chen et al., 2020; Werth and Avissar, 2004).

Inaccurate simulation of LAI can also contribute to the underestimation of LE. The ELM simulated mean daily LAI (4.7 - 4.8 m^2 m^{-2}) for 2018 and 2019 were in the range of satellite observations (3.9 - 4.9 m^2 m^{-2}) (Fig. S6, Griffis et al., 2020). However, the simulated LAI shows little seasonal variability throughout the year, which contrasts with satellite observations showing a slight increase in LAI during the dry seasons (Fig. S6). For example, the mean simulated LAI during the wet and dry seasons of 2019 were statistically not different ($p > 0.05$) with 4.76 and 4.77 m^2 m^{-2}, respectively; while for the observed LAI, mean wet and dry season LAI of 2019 were statistically different ($p < 0.05$) with 3.7 and 5.0 m^2 m^{-2}, respectively (Griffis et al., 2020). Recent studies have reported significant seasonal variation in LAI for Amazonian evergreen forests with evidence for higher LAI during the dry seasons caused by newly produced leaves (Wu et al., 2016, 2020). These new maturing leaves can drive a dry season increase in canopy photosynthesis and transpiration (Wu et al., 2016, 2020). Additional LAI measurement and phenological monitoring need to be conducted to quantify the phenological stages of dominant trees, i.e., *M. flexuosa* and *T. insignis*, for this site.

Another possible explanation is that the canopy leaves in this forest site were not realistically cooled during the daytime, given the single-layer canopy scheme implemented in the model. ELM simulated a single-layer canopy temperature (Tc) that was distinctly warmer around noontime and cooler after sunset when compared to the observed air temperature (Ta) (Fig. S7) and canopy temperature as derived from the sensible heat flux observations. The differences between Tc and Ta (ΔT) were more pronounced in the dry seasons than wet seasons (Fig. S7b, d). This implies that during the daytime, turbulent exchange and transpiration did not sufficiently remove the radiative heat load of the canopy, especially in the dry seasons. The differences between diel patterns of simulated Tc and Ta and the magnitude of ΔT (−1.92 - 1.85 °C) were consistent with some observations in tropical forests (Dong et al., 2017). However, some observational studies for tropical forests showed lower magnitude of ΔT and argued that only sunlit leaves in the upper canopy were warmer than Ta (Miller et al., 2021). Rey-Sánchez et al. (2016) observed that the mean Tc of two tropical tree species was significantly cooler than Ta by 0.7 - 0.8 °C during the dry seasons. Generally, the canopy air gradually cools by sensible heat transfer, and higher wind speeds in the canopy can produce stronger heat transfer. The cooling of leaves depends on canopy position: the upper canopy has higher wind speed and is generally cooler than the lower canopy during the daytime, despite receiving more radiation (Bonan et al., 2021). However, with the single-layer canopy scheme in ELM, and limited observations, we could not identify the vertical distribution of microclimates along the canopy height profiles. Some recent studies using single-layer LSMs for forest sites reported that the simple scheme is frequently insufficient to describe the surface conditions (e.g., temperature, humidity and wind speed) (Bonan et al., 2018; Song et al., 2021). In contrast, relative good agreement has been mostly reported for shorter croplands and grasslands (Bonan et al., 2018; Chen et al., 2015).

Large differences in LE and H between simulations and observations have been associated with the failure to vertically partition the incoming solar radiation realistically for the depth of the whole canopy. Moreover, the simplification for simulating within-canopy turbulent processes with the single-layer canopy scheme could also contribute to these biases. As in CLM4.5, ELM is based on the assumption of the Monin-Obukhov Similarity Theory that the within-canopy turbulent transfer is driven by diffusion gradient and can be described using eddy diffusivities. These models simplify the within-canopy wind speed by being equal to the canopy-top friction velocity and including a dynamic drag coefficient to describe the canopy stability condition (Bonan et al., 2021; Oleson et al., 2013). However, as Bonan et al. (2021) reviewed, this simple approach would bring bias when parameterizing turbulent fluxes between vegetation and the atmosphere, i.e., the definition of aerodynamic conductance, and consequently it is difficult to represent the turbulent flux within the tree canopy. Bonan et al. (2021) argued that using multi-layer canopy schemes with a Lagrangian profiling approach in LSMs can significantly reduce these known biases in turbulent energy fluxes and partitioning for forests. For example, compared to single-layer canopy simulation, their results in a deciduous broadleaf forest showed that multilayer canopy simulations can enhance the daytime cooling in the upper canopy and consequently suppress turbulent mixing. At the same time, during the night, the warmer temperature was better resolved in the upper canopy with greater turbulent mixing. For our research site, further vertical profile micrometeorological observations, e.g., air temperature, VPD, and CO_2 concentrations, would help improve these relevant model algorithms. This experimental and modeling work is ongoing.

3.3. Net ecosystem CO_2 exchange

Diel patterns of simulated CO_2 fluxes in both the wet and dry seasons are shown in Fig. 2g - h. ELM underestimated the peak diel CO_2 fluxes for each season, despite using the objective parameter optimization procedure (described in Section 2.3) for the photosynthesis-related parameters and using the improved algorithm describing the seasonality of leaf C/N ratio. For example, in 2019 the peak simulated diel CO_2 fluxes for the wet seasons were about −16.2 μmol m^{-2} s^{-1}, while the observations peaked at −20.4 μmol m^{-2} s^{-1}. During the dry seasons, observed and simulated diel CO_2 fluxes reached −16.3 μmol m^{-2} s^{-1} and −10.3 μmol m^{-2} s^{-1}, respectively. The underestimation of the observed diel CO_2 fluxes mainly occurred in the daytime from 9:00 to15:00 for both wet and dry seasons.

ELM showed similar seasonal CO_2 flux patterns as the observations with larger fluxes during the wet seasons and lower values during the dry seasons (Fig. 3d). For example, compared to the observations, the simulated fluxes during the wet season of 2019 were on average 38% lower at 1.82 μmol m^{-2} s^{-1}. ELM simulations and the observations indicated that the PE-QFR site was a carbon sink during the wet seasons. During the dry seasons, ELM simulations indicated the peatland was a weak net CO_2 source both in 2018 (0.1 μmol m^{-2} s^{-1}) and 2019 (0.8 μmol m^{-2} s^{-1}). However, the gap-filled observations indicated that the peatland was a weak net CO_2 sink (−0.5 μmol m^{-2} s^{-1} in 2018 and −0.03 μmol m^{-2} s^{-1} in 2019). From the Taylor diagram (Fig. 4d), we find that the model captured the amplitude of CO_2 fluxes well in both 2018 and 2019 with average $r = 0.85$, RMSE = 1.2 μmol m^{-2} s^{-1} and SD = 1.4 μmol m^{-2} s^{-1}. Compared with the simulated CO_2 fluxes in 2018 ($r = 0.81$, RMSE = 1.3 μmol m^{-2} s^{-1}, and SD = 1.3 μmol m^{-2} s^{-1}), ELM simulations in 2019 had higher r (0.89), smaller RMSE (1.2 μmol m^{-2} s^{-1}), and SD (1.6 μmol m^{-2} s^{-1}) values in better agreement with the observations.

The underestimation of net ecosystem CO_2 exchange is directly related to the simulations of GPP and ER. Figure S8 shows an underestimation of GPP compared to the observations (inferred from EC flux partitioning) following the parameter optimization and algorithm improvements. Further, there were some large differences in ER that occurred during the wet seasons, while slight overestimations of ER were found in the mornings of the dry seasons. Griffis et al. (2020) also suggested that the decline in GPP and the enhanced ER dominated the pattern of NEE during the dry seasons. However, the drivers of NEE seasonality are complex and remain uncertain for Amazonian forests. Our previous work found that high light, air temperature, and vapor pressure deficit (VPD) can significantly limit the photosynthesis rate in these tropical peatlands despite the relatively high water table position (Griffis et al., 2020). However, other Amazonian forest studies have

indicated that leaf development and demography also determine the GPP seasonality (Saleska et al., 2016; Wu et al., 2016). These research efforts show that the seasonality of NEE may be more complex than the current model structure of most LSMs. Furthermore, we should acknowledge the calculation uncertainties for the EC partitioned GPP and ER values. For example, this study's observed GPP and ER were estimated from a standardized NEE flux partitioning method that assumes the daytime ER follows the same relationship with environmental factors as the nighttime ER and uses a hyperbolic light-response method to estimate ER (Lasslop et al., 2010). Some studies have questioned the validity of these light-response partitioning methods because they adopt the same temperature sensitivity between daytime and nighttime and do not explicitly account for the Kok effect (Li et al., 2022; Zhang et al., 2006).

3.4. Net ecosystem CH_4 exchange

The improved ELM generally simulated diel CH_4 fluxes well, although with a slight overestimation around noontime during the wet seasons (Fig. 2i - j). During the wet seasons, ELM showed a pronounced peak during midday, whereas the observations revealed a smaller peak at this time. The simulated peak (73.8 nmol $m^{-2} s^{-1}$) was synchronous with, but slightly higher than, the observations (67.8 nmol $m^{-2} s^{-1}$). During the dry seasons the simulated and observed CH_4 fluxes had no distinct diel pattern. The variability in simulated CH_4 fluxes across days was much smaller than observed in both the wet and dry seasons. The average simulated daily CH_4 fluxes during the wet season were 50.6 nmol $m^{-2} s^{-1}$, 83.9% higher than the dry seasons (27.5 nmol $m^{-2} s^{-1}$).

An identifiable seasonal shift in CH_4 fluxes was captured by ELM (Fig. 3e). The simulated daily CH_4 fluxes had higher values during the wet seasons. Overall, ELM simulated that the site was a net CH_4 source over the whole year, consistent with the observations. In 2019, the ELM simulated seasonal maximum CH_4 fluxes occurred in March, reaching 56.2 nmol $m^{-2} s^{-1}$. Minimum emissions were simulated in November (20.5 nmol $m^{-2} s^{-1}$). In the observations, maximum (116.8 nmol $m^{-2} s^{-1}$) and minimum (9.6 nmol $m^{-2} s^{-1}$) CH_4 fluxes occurred in February and November, respectively. Overall, the simulated seasonal pattern of daily CH_4 fluxes did not represent the observed seasonal pattern of emissions. The seasonal variability of simulated CH_4 fluxes was lower than the observations in both the wet (71.0 nmol $m^{-2} s^{-1}$ for observations, 50.5 nmol $m^{-2} s^{-1}$ for simulation) and dry seasons (33.5 nmol $m^{-2} s^{-1}$ for observations, 27.7 nmol $m^{-2} s^{-1}$ for simulation). On the other hand, the Taylor diagram (Fig. 4e) indicates that simulated CH_4 fluxes compared well with the observations (r = 0.79, RMSE=17.5 nmol $m^{-2} s^{-1}$). However, the simulated SD (11.5 nmol $m^{-2} s^{-1}$) was considerably smaller than the observed values (19.1 nmol $m^{-2} s^{-1}$), indicating that the model did not capture all of the short-term dynamics of CH_4 exchange. The simulated weaker seasonal variability of CH_4 emissions in tropical wetlands compared to other regions was also noted in a CLM4.5 modeling study (Meng et al., 2015).

Compared to the total net ecosystem CH_4 exchange (Fig. 3e), the simulated CH_4 fluxes *via* diffusion, ebullition, and plant transport exhibited a similar seasonal dynamic in the Amazonian palm swamp peatland - high during the wet seasons and low during the dry seasons (Fig. 5a). The same seasonal patterns of diffusive, ebullition and tree CH_4 fluxes have been reported previously for field observations for peatlands in the Peruvian Amazon (Pangala et al., 2017; Teh et al., 2017); however, some observational studies have found low seasonal variability of tree CH_4 fluxes near this site (van Haren et al., 2021). The divergent seasonal trends may be linked to the interannual variations in environmental drivers (van Haren et al., 2021). Further, unrealistic modeling schemes in LSMs may also underlie the different performances (discussed below).

The total simulated annual CH_4 budget was 16.04 ± 4.47 g C m^{-2}

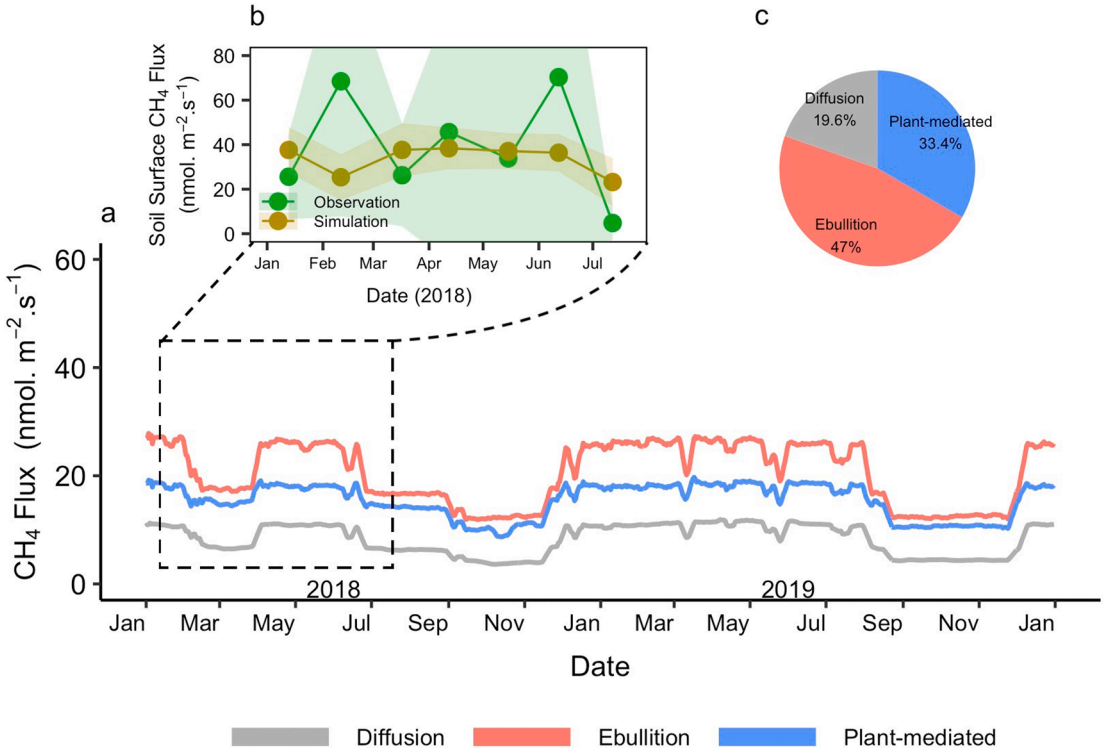

Fig. 5. The seasonal patterns of simulated daily (5-day moving average) CH_4 transport pathways in 2018 and 2019 (a). b presents a zoom of the plot for simulated midmonthly soil surface CH_4 fluxes (by summing the simulated CH_4 fluxes of soil diffusion and ebullition) in the period January 15 to July 15 of 2018, with corresponding soil chamber observations from Hergoualc'h et al. (2020) (Shaded error bars represent standard deviation). The pie chart shows the total contribution for each pathway to the annual sum of CH_4 emissions (c).

year^{-1} (mean ± SD, similarly hereafter) and was 27.1% lower than the observed budget of 22 ± 2 g C m $^{-2}$ year^{-1} (Griffis et al., 2020). The simulated CH_4 flux components of plant transport, soil diffusion, and ebullition during the dry seasons were 49.9%, 41.3%, and 61.0% lower than during the wet seasons, respectively. The simulated CH_4 flux components of ebullition, plant transport, and soil diffusion contributed 47.0%, 33.4%, and 19.6% to the annual total CH_4 fluxes, respectively (Fig. 5c). Compared with field measurements of soil surface CH_4 fluxes from January to July of 2018 at this site (data from Hergoualc'h et al., 2020), the ELM sums of soil diffusion and ebullition CH_4 fluxes were on average overestimated by about 51 ± 153% (−43.1 - 18.4 nmol m $^{-2}$ s $^{-1}$) (Fig. 5b). This implies that the plant-mediated CH_4 transport might also be underestimated by 51% for this same period given that there is reasonably good agreement between ELM and the EC CH_4 budget. However, the magnitude of divergence varied by month but no apparent seasonality, and the underestimation may be larger than our estimations because the soil chambers can also partially capture root-mediated CH_4 transport.

We hypothesize that the underestimation of the annual CH_4 emissions by ELM compared to observations was caused by the poor simulation of the plant-mediated CH_4 transport for tropical palms. This is because the CH_4 diffusive fluxes are described with Fick's Law and Henry's Law, and ebullition is described using a bubbling threshold approach (CH_4 concentration, pressure, or gas volume threshold) (Ma et al., 2021; Ricciuto et al., 2021; Riley et al., 2011), which are both abiotic physical processes and have been widely observed and well tested (Riley et al., 2011; Xu et al., 2015). In contrast, the transport of CH_4 through the aerenchyma of vascular plants in ELM is calculated from soil CH_4 gas concentration with one plant-mediated transport parameter (*m_dPlantTrans*) and two root parameters (*Rootp* and *RootFactor*) (Ricciuto et al., 2021; Xu et al., 2015). This approach does not include plant non-aerenchymatous transport mechanisms yet, such as the transport via stems (see Section 3.6). Our sensitivity analyses also indicated that the simulated total CH_4 fluxes were less sensitive to *m_dPlantTrans* and root depth distribution parameters (see Section 3.5). In addition, several recent studies in Amazonian regions have reported that the stems of woody trees can act as an important pathway for the CH_4 transport (Pangala et al., 2017). Griffis et al. (2020) also suggested the potential importance of the plant-mediated CH_4 transport at the site according to the observed relationships between CH_4 emissions and LE and CO_2 fluxes (i.e., *via* a surrogate relation for transpiration). Therefore, the estimation bias in the CH_4 fluxes may be related to the model structure given the simple empirical approach representing the plant-mediated CH_4 fluxes for the Amazonian palm swamp peatland. Recent experiments have been initiated at the PE-QFR site to further investigate these mechanisms.

3.5. Parameter controls on energy and carbon exchange

Fig. 6 represents the main effect sensitivity indices of model output variables to 21 particular parameters, indicating diverse parameter contributions to the simulation variance during different seasons. For the energy exchange, the processes of vegetation phenology (*fcur* and *leaf_long*), stomatal regulation of transpiration (*mp*), and nitrogen-photosynthesis relationship (*flnr*) were generally very important (Fig. 6a). However, different impacts of parameters on energy fluxes

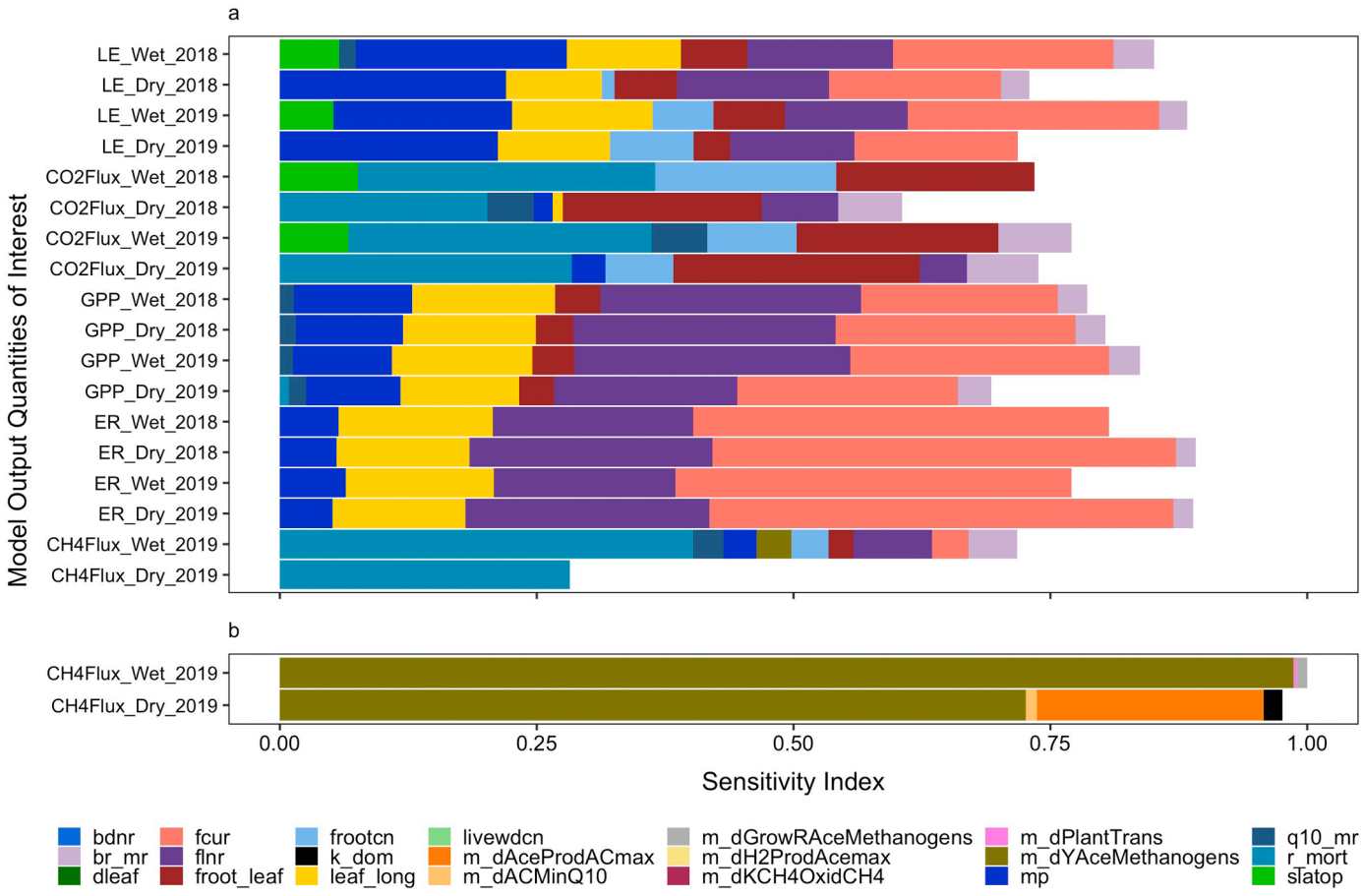

Fig. 6. Sensitivity analysis of 21 screened parameters (Table 1) for latent heat fluxes (LE), gross primary production (GPP), ecosystem respiration (ER), CO_2 fluxes, and CH_4 fluxes (a). All output variables represent the average values of wet and dry seasons in 2018 and 2019. Figure b illustrates the independent sensitivities of CH_4 fluxes controlled by microbial parameters (for which parameters begin with 'm_'). The width of each bar represents the main effect sensitivity index (Sobol index) for each parameter.

exist across seasons at the PE-QFR site. During the wet seasons, vegetation phenology (*fcur*) contributed to LE more than the stomatal regulation parameter (*mp*), while the contribution from *mp* was larger than *fcur* during the dry seasons. This indicates that a trade-off between vegetation phenology (*fcur*) and physiology (*mp*) likely exists in this ecosystem. Renninger and Phillips (2011) suggested that *M. flexuosa* can exhibit similar capacities for water transport per unit leaf area under different water conditions with differing hydraulic strategies. Our previous work observed that increased VPD during the dry seasons was associated with a down regulation of photosynthesis (Griffis et al., 2020), which may be due to the hydraulic regulation of stomata. Besides the model structure errors (Section 3.2), the vegetation hydraulic strategies might also contribute to the changes of CO_2 fluxes and LE during the dry seasons. The strong dependence of energy exchange on *leaf_long* also highlights the importance of leaf phenology. From 2018 to 2019, significant interannual changes in parameter controls on energy exchange were found as well because of the physiological plasticity of tropical vegetation in response to different growth environments. For example, in contrast to the dry season of 2018, the impact of fine root C:N ratio (*frootcn)* on LE was enhanced in the dry season of 2019, reflecting changing impacts of new fine root growth associated with different nutrient allocation strategies, perhaps due to the short dry season for green-up in 2019 (Dry season duration: 61 days of 2019 *vs* 153 days of 2018). Indeed, for the PE-QFR site, it was found that fine root productivity rate of *M. flexuosa* palm tends to increase linearly with rising soil temperature, while fine root mortality tends to decrease linearly with increased water table level (Dezzeo et al., 2021).

In contrast to energy fluxes, no apparent seasonal or interannual differences in the relative sensitivity of CO_2 fluxes to specific parameters were found (Fig. 6a). The variance of CO_2 fluxes mainly depended on vegetation mortality rate (*r_mort*), fine root to leaf allocation ratio (*froot_leaf*), and fine root C:N ratio (*frootcn*). However, similar to energy fluxes, GPP and ER were most sensitive to *fcur, mp, flnr* and *leaf_long*. The most sensitive parameters for GPP and ER were *flnr* and *fcur*, respectively. Although we did not test the sensitivity of the leaf C/N ratio in the revised model, the better seasonal performance of CO_2 fluxes with the new leaf C/N ratio function indicates its importance for the seasonality of GPP. Previous studies have observed considerable age-related variation in leaf traits including leaf nitrogen/carbon in Amazonian forests and found that leaf nitrogen increases by 20 - 25% during the dry seasons in Amazonian floodplains with the flush of new leaves (Chavana-Bryant et al., 2017; Parolin et al., 2002), which contributes significantly to the seasonality of GPP (Wu et al., 2016, 2020).

There was significant seasonal variability in the most sensitive parameters for CH_4 fluxes. The sensitivity to plant- and soil-related parameters was higher than for microbial parameters (Fig. 6a). During the wet seasons, CH_4 fluxes were most sensitive to three key plant-related parameters including *r_mort, flnr*, and the plant maintenance respiration parameter (*br_mr*). During the dry seasons, *r_mort* was a single key parameter associated with the variations in CH_4 fluxes. The seasonal parameter variability controlling CH_4 fluxes is related to the seasonal changes in plant activities. Plants regulate carbon flux dynamics, including the carbon input of litter and root exudates for peat formation. They also control gas transport (i.e., oxygen, CH_4) between the atmosphere and soil/water through their pneumatophore system (van Lent et al., 2019). However, in a global simulation study using CLM4.5, CH_4 emissions in tropical wetlands were more sensitive to the soil substrate production represented by heterotrophic respiration (Paudel et al., 2016). Such difference in parameter sensitivity is likely caused by the different CH_4 biogeochemical schemes and diverse ecosystem characteristics. For example, compared to CLM4.5, ELM adds additional process complexity through its representation of explicit methanogenic pathways and microbial populations (Ricciuto et al., 2021).

Our independent sensitivity analysis on microbial controls for CH_4 fluxes also represented the seasonal variation in relative parameter importance (Fig. 6b). It illustrates that CH_4 fluxes were mostly dominated by the growth efficiency of acetoclastic methanogens (*m_dYAceMethanogens*) during the wet seasons. During the dry seasons, in addition to *m_dYAceMethanogens*, CH_4 fluxes were also very sensitive to the maximum acetic acid production rate (*m_dAceProdACmax*). Acetoclastic methanogenesis is generally considered to be the main CH_4 production pathway in temperate and boreal peatlands (Xu et al., 2016), while some studies have indicated that hydrogenotrophic methanogenesis can be responsible for $>$ 50% of the CH_4 production in tropical peatlands (Holmes et al., 2015). One recent microbial community structure study also suggested that hydrogenotrophic methanogenesis is the primary source of CH_4 in seven peatlands from the Pastaza-Marañón Basin (Finn et al., 2020). However, our sensitivity analyses did not identify a high sensitivity of hydrogen (H_2) consumption parameter *m_dH2ProdAcemax* (the maximum reaction rate of conversion of H_2 and CO_2 to acetic acid), although the values of acetoclastic methanogenesis parameters *m_dAceProdACmax* and *m_dYAceMethanogens* were reduced after optimization. Future parameter sensitivity analyses and optimization for this Amazonian palm swamp peatland need to include hydrogenotrophic-methanogenesis-related parameters, such as the growth rate and temperature sensitivity of hydrogenotrophic methanogens. Because the conversation of H_2 produced through fermentation of carbohydrates to acetic acid and CH_4 also depends on the concentration of H_2 (Xu et al., 2015) and pH condition (Finn et al., 2020), the threshold parameters of H_2 concentration and pH condition also need to be considered. Here, we did not find a strong impact of plant-mediated CH_4 transport (*m_dPlantTrans*) on the variability in CH_4 emissions for all seasons. However, the results above indicate that plant-related parameters have potential contributions to CH_4 plant transport. We acknowledge that the parameter sensitivity analysis cannot provide insights into parameters or processes that are missing from the model structure. For example, Fig 6 shows that CH_4 fluxes were most sensitive to only a few key parameterizations, indicating that some CH_4 processes in current ELM that are either not fully understood or not captured with current posterior parameter ranges. As described above (Sections 3.2, 3.3 and 3.4), the model algorithms for energy and CO_2 fluxes and plant-mediated CH_4 fluxes may need to be further improved. These model analyses are being used to inform ongoing experiments at the research site.

As expected, we found that the parameters for the fraction of nitrogen allocated to RuBisCO enzyme (*flnr*) and the Ball–Berry stomatal conductance slope (*mp*) were both important to the energy and carbon fluxes for the PE-QFR site. This is consistent with numerous studies on terrestrial ecosystems with CLM and the previous versions of ELM (Fan et al., 2015; Ricciuto et al., 2018; Shi et al., 2021; Yuan et al., 2021b). This is because *flnr* determines the nitrogen use strategies of leaf carbon assimilation and affects the development of leaf area, and *mp* determines the leaf energy loss from transpiration and carbon photosynthesis and respiration by controlling stomal conductance in the model. Our study also highlights the importance of the parameters related to photosynthetic phenology for the Amazonian palm swamp peatland, such as the parameters of *fcur* and *br_mr,* which control the photosynthetic efficiency in the model, and *leaf_long* and *r_mort*, which control the timing of vegetation activity (i.e., vegetation mortality rate, *r_mort*, was the most sensitive parameter for the variance of CO_2 fluxes in Fig. 6a). Several global modeling studies have also identified the significant impacts of these parameters on photosynthetic capacity and phenological timing (Kolassa et al., 2020; Ricciuto et al., 2018). Further, Ricciuto et al. (2018) also found that in ELM the sensitive parameters for tropical carbon cycling are mostly associated with vegetation processes. For example, the leaf area in tropical broadleaf evergreen sites is very sensitive to the leaf longevity (*leaf_long*) and the base rate of maintenance respiration (*br_mr*).

For the energy and carbon fluxes, the temperature controls on vegetation processes also need to be considered. Temperature regulates respiratory CO_2 release *via* two alternative and cytochrome pathways of mitochondrial electron transport chain. The temperature-respiration

relationship is represented by the widely used temperature coefficient Q_{10}. For example, maintenance respiration is used for satisfying the metabolic needs for existing mature cells, whose temperature sensitivity refers to the parameter *q10_mr* in ELM. Temperature also affects photosynthetic CO_2 - fixation directly through modulation of activity of photosynthetic enzymes and the electron transport chain of the light reactions, and indirectly by controlling the stomatal conductance through VPD. In most ecosystem models, including ELM, the peaked Arrhenius model is used to describe the instantaneous temperature response of respiration and photosynthesis, and to calculate the optimum temperatures of V_{cmax} and J_{max}. Tan et al. (2017) found strong VPD and stomatal limitation on optimum air temperature for tropical forests, which implies that the temperate dependency of tropical forests can change during different seasons. However, the values of key photosynthesis parameters in most LSMs have been derived mainly from northern temperate and boreal trees and have lacked tropical species (Lombardozzi et al., 2015). The discrepancies in energy fluxes may be related to the simulations of canopy water-vapor conductance, which is strongly temperature dependent.

We hypothesized that the plant root system would have a strong influence on the carbon exchange in this Amazonian palm swamp peatland. Larger palms may have more extensive or deeper roots and have a relatively lower rhizosphere oxygenation due to higher oxygen consumption with more root respiration, which consequently limits CH_4-oxidation and causes increased local soil CH_4 concentrations (van Haren et al., 2021). However, we showed that the root depth distribution parameters *roota* and *rootb* were found to be less sensitive to both CO_2 and CH_4 fluxes. Therefore, *roota* and *rootb* were omitted from the most-sensitive-parameter list after the parameter downselection (Tables 1 and S1), which indicates that root distribution may not be the limiting factors for the carbon dynamics in the PE-QFR site. Perhaps this is because the dominant tree species *M. flexuosa* is known to have a shallow rooting system with more lateral root growth. Investigations on the root biomass in this study area suggest that species growing in these palm swamp forests are very tolerant to high water table and saturated soil conditions (Dezzeo et al., 2021).

For wetland simulations, the anaerobic environment is crucial for CH_4 production and oxidation. It is mainly controlled by water table level and microtopography. To improve the hydrological controls on carbon cycle processes in ELM for the Amazonian palm swamp peatland, we modified the model algorithms of the soil water retention curve and water coverage scalar function. The improved simulations showed that the seasonal variation of simulated CH_4 emissions followed the changes of water table position during the wet and dry seasons (Fig. S9). In our previous study of a boreal forest peatland, the simulated CH_4 emissions were sensitive to surface water drainage rate and soil water potential parameters (Yuan et al., 2021a). However, in this Amazonian palm swamp peatland we did not find high sensitivity of CH_4 emissions to these hydraulic parameters. One possible explanation is that the site is always waterlogged and the soil is near saturation for the entire year, which favors peat development.

In addition, we found that there were pronounced interactions of the 21 parameters for carbon fluxes in different seasons (Joint total sensitivity index >1, Fig. S10), but smaller sensitivity of ecosystem respiration (ER) to the parameter interactions. However, the joint total effects on most QoIs did not exhibit regular seasonal and interannual variability. Although some parameters showed negligible main effects for some QoIs in different seasons, they have shown sensitivities when interacting with each other. For example, the main effect of canopy leaf area distribution (*slatop*) showed that it was not important to the energy and carbon fluxes, while its joint parameter interactions were significant for LE (with *mp* and *fcur*) and CO_2 fluxes (with *frootcn* and *q10_mr)* in both wet and dry seasons, and CH_4 fluxes (with *fcur*) in wet seasons (Fig. S11). This further indicates the importance of vegetation phenology and physiology processes to the Amazonian palm swamp peatland.

3.6. Limitations and future work

Our study provides an important early step in improving the understanding of carbon dynamics of Amazonian peatlands through a model-measurement approach. A few limitations remain in ELM when predicting the energy and carbon fluxes of this peatland and will be addressed as additional data become available for the PE-QFR research site.

Here, the model optimization was carried out by using a parameter sensitivity analysis given the scarcity of field observations. A potential limitation, therefore, is the limited range of parameter values from tropical peatland sites. The parameter ranges defined here were not the specific values for the Amazonian palm swamp peatland, but defined by the global values from published papers, physically constrained, +/− 50% of the default value, or based on expert judgment. In addition, the improved functions of soil water retention and leaf carbon-to-nitrogen ratio assume the same behaviors exhibited in the PE-QFR site as other tropical peatlands. Detailed soil physical and plant physiological data also need to be investigated for this site.

We employed a simple empirical function of the leaf C/N ratio with aging to describe the seasonality of CO_2 fluxes. This approach may lack a universal mechanism for its application to other Amazonian peatlands. Further improvements on leaf phenological simulations still need to be carried out with support from leaf physiological measurements and more clear understanding of the drivers. In the model settings, only a single plant functional type of default tropical broadleaf evergreen tree was defined. However, different development stages were found among tropical broadleaf evergreen tree species. For example, palms can sustain a high level of LAI while producing fruits continuously (Fan et al., 2015), which may alter LAI development and carbon allocation processes compared to other tree species. More field LAI and phenological observations may reduce these potential modeling uncertainties.

The underlying mechanisms of plant-mediated CH_4 transport in the Amazonian palm swamp peatland need to be further investigated in future experimental and modeling work. Large contributions to CH_4 transport from stem/shoot transport have been observed for tropical peatlands (Pangala et al., 2017; Teh et al., 2017; van Haren et al., 2021), and the contributions of different plant-tissue pathways vary widely across tree species (Covey and Megonigal, 2019; Putkinen et al., 2021). Future synchronized high-frequency CH_4 measurements and lab-based analysis of taxonomic and functional microbes for both soil and tree organs should be used to help identify and address detailed CH_4 production and consumption processes (Covey and Megonigal, 2019; Putkinen et al., 2021). This would also be useful for development of the algorithm for microbial-based plant-mediated CH_4 transport. In addition, inventories of tree architectural variables, e.g., stem diameter, tree height and crown width, will be useful for scaling the tree CH_4 emissions to the ecosystem level. Moreover, we did not identify the effects of hollows and hummocks, and only roughly assessed the site-level soil CH_4 fluxes by averaging all relevant soil CH_4 flux chamber data from Hergoualc'h et al. (2020) (Fig 5). However, Hergoualc'h et al. (2020) suggested that the soil CH_4 fluxes were affected by the microtopography associated with hollows and hummocks within the study area. This may be why we found that the discrepancy between simulated and observed soil CH_4 fluxes varied over months. Further modeling studies to capture the spatial heterogeneity of CH_4 fluxes caused by the microtopographic differences in the peatland are still needed.

Peatlands are often regarded as stable systems and act as a net cooling mechanism for Earth's climate (Frolking et al., 2006). Some modeling studies indicate that boreal peatlands will lose significant carbon in the future due to projected permafrost thaw under climate change (Loisel et al., 2021). However, the fate of peat carbon storage in the tropics remains highly uncertain (Ribeiro et al., 2021; Zhang et al., 2017). The water balance is recognized as the main factor driving the peat accumulation for most peatlands (Kurnianto et al., 2015). The Sixth Assessment Report (AR6) from the Intergovernmental Panel on Climate

Change (IPCC) indicates that there will be less precipitation in the northwest Amazon (Iturbide et al., 2020). However, some predictions suggested higher precipitation for the region (Marengo and Espinoza, 2016), highlighting the inherent uncertainty in these projections. In general, severe drought induces peatland degradation and carbon loss (Loisel et al., 2021). With robust tropics-specific peatland models, we can better understand how the carbon budget and detailed carbon cycle processes in the Amazonian palm swamp peatland will respond to climate variability and future climate change (Hergoualc'h et al., 2020). Therefore, improving the forecasting capability for this tropics-specific model is still urgently needed.

4. Conclusions

In the study, we evaluated the performance of ELM for simulating energy and carbon fluxes in an Amazonian palm swamp peatland. Several key algorithms were modified according to site-specific characteristics. An objective parameter optimization approach with a surrogate-assisted Bayesian methodology was used to optimize ELM. The modified functions included the soil water retention curve, water coverage scalar function in CH_4 processes, and seasonally varying leaf carbon-to-nitrogen ratio function. The optimized tropics-specific model showed significantly improved simulations for the seasonal and diel patterns of energy and carbon fluxes for this tropical peatland. However, some biases in the simulated fluxes remain and require further research. Specifically, these include the underestimations for LE and overestimation of H during the dry seasons, the underestimation of CO_2 fluxes in the daytime, and the low seasonal variability of CH_4 fluxes. Parameter sensitivity analyses indicated that the strong controls on energy and carbon fluxes were mainly attributed to parameters associated with vegetation activities, such as plant carbon distribution, stomatal regulation, photosynthesis-nitrogen relationship, and leaf phenology. These sensitivities and the controls changed in different periods (i.e., wet vs dry seasons). This modeling study expanded the applicability of the ELM model in tropical peatlands, advanced our understanding of biotic controls on the energy and carbon exchange of the Amazonian palm swamp peatland and identified knowledge gaps that need to be addressed for better prediction of carbon processes and budgets for tropical peatlands, e.g., the modeling bias due to the lack of ability to simulate CH_4 transport from non-aerenchymatous tissues in current model.

Declaration of Competing Interest

The authors declare that there is no conflict of interest regarding the publication of this paper.

Data availability

Observational data are available through the AmeriFlux network at: https://ameriflux.lbl.gov/sites/siteinfo/PE-QFR. ERA5 data can be downloaded from the Climate Data Store (CDS) at https://www.ecmwf.int/en/forecasts/datasets/reanalysis-datasets/era5. Original ELM-SPRUCE code is available on the Github repository at https://github.com/dmricciuto.

Acknowledgements

This study was supported by the Office of Biological and Environmental Research in the Department of Energy Office of Science (DE-SC0020167). Other financial supports include the Sustainable Wetlands Adaptation and Mitigation Program (SWAMP, Grant MTO-069018) by the United States of America and the Global Comparative Study on REDD + (Grant agreement #QZA-12/0882) by the Government of Norway. This study used the computing resources provided by the Minnesota Supercomputing Institute (MSI) at the University of Minnesota. We also acknowledge two anonymous reviewers for their insightful comments and suggestions that significantly improved the manuscript.

Supplementary materials

Supplementary material associated with this article can be found, in the online version, at doi:10.1016/j.agrformet.2023.109364.

References

Baker, J.C., Garcia-Carreras, L., Gloor, M., Marsham, J.H., Buermann, W., da Rocha, H. R., Nobre, A.D., de Araujo, A.C., Spracklen, D.V., 2021. Evapotranspiration in the Amazon: spatial patterns, seasonality, and recent trends in observations, reanalysis, and climate models. Hydrol. Earth Syst. Sci. 25, 2279–2300.

Bhomia, R.K., van Lent, J., Rios, J.M.G., Hergoualc'h, K., Coronado, E.N.H., Murdiyarso, D., 2019. Impacts of Mauritia flexuosa degradation on the carbon stocks of freshwater peatlands in the Pastaza-Marañón river basin of the Peruvian Amazon. Mitig. Adapt. Strateg. Glob. Chang. 24, 645–668.

Bonan, G.B., Patton, E.G., Finnigan, J.J., Baldocchi, D.D., Harman, I.N., 2021. Moving beyond the incorrect but useful paradigm: reevaluating big-leaf and multilayer plant canopies to model biosphere-atmosphere fluxes–a review. Agric. For. Meteorol. 306, 108435.

Bonan, G.B., Patton, E.G., Harman, I.N., Oleson, K.W., Finnigan, J.J., Lu, Y., Burakowski, E.A., 2018. Modeling canopy-induced turbulence in the Earth system: a unified parameterization of turbulent exchange within plant canopies and the roughness sublayer (CLM-ml v0). Geosci. Model. Dev. 11, 1467–1496.

Bridgham, S.D., Cadillo-Quiroz, H., Keller, J.K., Zhuang, Q., 2013. Methane emissions from wetlands: biogeochemical, microbial, and modeling perspectives from local to global scales. Glob. Chang. Biol. 19, 1325–1346.

Carswell, F., Meir, P., Wandelli, E., Bonates, L., Kruijt, B., Barbosa, E.M., Nobre, A., Grace, J., Jarvis, P., 2000. Photosynthetic capacity in a central Amazonian rain forest. Tree Physiol. 20, 179–186.

Chavana-Bryant, C., Malhi, Y., Wu, J., Asner, G.P., Anastasiou, A., Enquist, B.J., Cosio Caravasi, E.G., Doughty, C.E., Saleska, S.R., Martin, R.E., 2017. Leaf aging of Amazonian canopy trees as revealed by spectral and physiochemical measurements. New Phytol. 214, 1049–1063.

Chen, M., Griffis, T.J., Baker, J., Wood, J.D., Xiao, K., 2015. Simulating crop phenology in the Community Land Model and its impact on energy and carbon fluxes. J. Geophys. Res. 120, 310–325.

Chen, X., Maignan, F., Viovy, N., Bastos, A., Goll, D., Wu, J., Liu, L., Yue, C., Peng, S., Yuan, W., 2020. Novel representation of leaf phenology improves simulation of Amazonian evergreen forest photosynthesis in a land surface model. J. Adv. Model. Earth Syst. 12, e2018MS001565.

Covey, K.R., Megonigal, J.P., 2019. Methane production and emissions in trees and forests. New Phytol. 222, 35–51.

Dean, J.F., Middelburg, J.J., Röckmann, T., Aerts, R., Blauw, L.G., Egger, M., Jetten, M. S., de Jong, A.E., Meisel, O.H., Rasigraf, O., 2018. Methane feedbacks to the global climate system in a warmer world. Rev. Geophys. 56, 207–250.

Dezzeo, N., Grandez-Rios, J., Martius, C., Hergoualc'h, K., 2021. Degradation-driven changes in fine root carbon stocks, productivity, mortality, and decomposition rates in a palm swamp peat forest of the Peruvian Amazon. Carbon Balance Manage. 16, 1–14.

Dong, N., Prentice, I., Harrison, S.P., Song, Q., Zhang, Y., 2017. Biophysical homoeostasis of leaf temperature: a neglected process for vegetation and land-surface modelling. Global Ecol. Biogeogr. 26, 998–1007.

Fan, Y., Roupsard, O., Bernoux, M., Le Maire, G., Panferov, O., Kotowska, M.M., Knohl, A., 2015. A sub-canopy structure for simulating oil palm in the Community Land Model (CLM-Palm): phenology, allocation and yield. Geosci. Model. Dev. 8, 3785–3800.

Farmer, J., Matthews, R., Smith, J.U., Smith, P., Singh, B.K., 2011. Assessing existing peatland models for their applicability for modelling greenhouse gas emissions from tropical peat soils. Curr. Opin. Environ. Sustain. 3, 339–349.

Finn, D.R., Ziv-El, M., Van Haren, J., Park, J.G., del Aguila-Pasquel, J., Urquiza–Muñoz, J.D., Cadillo-Quiroz, H., 2020. Methanogens and methanotrophs show nutrient-dependent community assemblage patterns across tropical peatlands of the Pastaza-Maranon Basin. Front. Microbiol. 11, 746.

Frolking, S., Roulet, N., Fuglestvedt, J., 2006. How northern peatlands influence the Earth's radiative budget: sustained methane emission versus sustained carbon sequestration. J. Geophys. Res. 111.

Ghanem, R., Higdon, D., Owhadi, H., 2016. The Uncertainty Quantification Toolkit (UQTk). Handbook of Uncertainty Quantification. Springer.

Griffis, T.J., Roman, D., Wood, J.D., Deventer, J., Fachin, L., Rengifo, J., Del Castillo, D., Lilleskov, E., Kolka, R., Chimner, R., 2020. Hydrometeorological sensitivities of net ecosystem carbon dioxide and methane exchange of an Amazonian palm swamp peatland. Agric. For. Meteorol. 295, 108167.

Gumbricht, T., Roman-Cuesta, R.M., Verchot, L., Herold, M., Wittmann, F., Householder, E., Herold, N., Murdiyarso, D., 2017. An expert system model for mapping tropical wetlands and peatlands reveals South America as the largest contributor. Glob. Chang. Biol. 23, 3581–3599.

Hergoualc'h, K., Dezzeo, N., Verchot, L.V., Martius, C., van Lent, J., del Aguila-Pasquel, J., Lopez Gonzales, M., 2020. Spatial and temporal variability of soil N_2O

and CH_4 fluxes along a degradation gradient in a palm swamp peat forest in the Peruvian Amazon. Glob. Chang. Biol. 26, 7198–7216.
Holmes, M.E., Chanton, J.P., Tfaily, M.M., Ogram, A., 2015. CO_2 and CH_4 isotope compositions and production pathways in a tropical peatland. Glob. Biogeochem. Cycles 29, 1–18.
Iiyama, I., Osawa, K., Nagai, T., 2012. A seasonal behavior of surface soil moisture condition in a reclaimed tropical peatland. Soil Sci. Plant Nutr. 58, 543–552.
Iturbide, M., Gutiérrez, J.M., Alves, L.M., Bedia, J., Cerezo-Mota, R., Cimadevilla, E., Cofiño, A.S., Di Luca, A., Faria, S.H., Gorodetskaya, I.V., 2020. An update of IPCC climate reference regions for subcontinental analysis of climate model data: definition and aggregated datasets. Earth Syst. Sci. Data 12, 2959–2970.
Kolassa, J., Reichle, R.H., Koster, R.D., Liu, Q., Mahanama, S., Zeng, F.W., 2020. An observation-driven approach to improve vegetation phenology in a global land surface model. J. Adv. Model. Earth Syst. 12, e2020MS002083.
Kurnianto, S., Warren, M., Talbot, J., Kauffman, B., Murdiyarso, D., Frolking, S., 2015. Carbon accumulation of tropical peatlands over millennia: a modeling approach. Glob. Chang. Biol. 21, 431–444.
Largeron, C., Krinner, G., Ciais, P., Brutel-Vuilmet, C., 2018. Implementing northern peatlands in a global land surface model: description and evaluation in the ORCHIDEE high-latitude version model (ORC-HL-PEAT). Geosci. Model. Dev. 11, 3279–3297.
Lasslop, G., Reichstein, M., Papale, D., Richardson, A.D., Arneth, A., Barr, A., Stoy, P., Wohlfahrt, G., 2010. Separation of net ecosystem exchange into assimilation and respiration using a light response curve approach: critical issues and global evaluation. Glob. Chang. Biol. 16, 187–208.
Li, N., Shao, J., Zhou, G., Zhou, L., Du, Z., Zhou, X., 2022. Improving estimations of ecosystem respiration with asymmetric daytime and nighttime temperature sensitivity and relative humidity. Agric. For. Meteorol. 312, 108709.
Lilleskov, E., McCullough, K., Hergoualc'h, K., del Castillo Torres, D., Chimner, R., Murdiyarso, D., Kolka, R., Bourgeau-Chavez, L., Hribljan, J., del Aguila Pasquel, J., Wayson, C., 2019. Is Indonesian peatland loss a cautionary tale for Peru? A two-country comparison of the magnitude and causes of tropical peatland degradation. Mitig. Adapt. Strateg. Glob. Chang. 24, 591–623.
Loisel, J., Gallego-Sala, A.V., Amesbury, M.J., Magnan, G., Anshari, G., Beilman, D.W., Benavides, J.C., Blewett, J., Camill, P., Charman, D.J., Chawchai, S., Hedgpeth, A., Kleinen, T., Korhola, A., Large, D., Mansilla, C.A., Muller, J., van Bellen, S., West, J. B., Yu, Z., Bubier, J.L., Garneau, M., Moore, T., Sannel, A.B.K., Page, S., Valiranta, M., Bechtold, M., Brovkin, V., Cole, L.E.S., Chanton, J.P., Christensen, T. R., Davies, M.A., De Vleeschouwer, F., Finkelstein, S.A., Frolking, S., Galka, M., Gandois, L., Girkin, N., Harris, L.I., Heinemeyer, A., Hoyt, A.M., Jones, M.C., Joos, F., Juutinen, S., Kaiser, K., Lacourse, T., Lamentowicz, M., Larmola, T., Leifeld, J., Lohila, A., Milner, A.M., Minkkinen, K., Moss, P., Naafs, B.D.A., Nichols, J., O'Donnell, J., Payne, R., Philben, M., Piilo, S., Quillet, A., Ratnayake, A. S., Roland, T.P., Sjogersten, S., Sonnentag, O., Swindles, G.T., Swinnen, W., Talbot, J., Treat, C., Valach, A.C., Wu, J., 2021. Expert assessment of future vulnerability of the global peatland carbon sink. Nat. Clim. Chang. 11, 70. -+.
Lombardozzi, D.L., Bonan, G.B., Smith, N.G., Dukes, J.S., Fisher, R.A., 2015. Temperature acclimation of photosynthesis and respiration: a key uncertainty in the carbon cycle-climate feedback. Geophys. Res. Lett. 42, 8624–8631.
Ma, S., Jiang, L., Wilson, R.M., Chanton, J.P., Bridgham, S., Niu, S., Iversen, C.M., Malhotra, A., Jiang, J., Lu, X., 2021. Evaluating alternative ebullition models for predicting peatland methane emission and its pathways via data-model fusion. Biogeosci. Discussions 1–30.
Marengo, J.A., Espinoza, J.C., 2016. Extreme seasonal droughts and floods in Amazonia: causes, trends and impacts. Int. J. Climatol. 36, 1033–1050.
Melton, J.R., Wania, R., Hodson, E.L., Poulter, B., Ringeval, B., Spahni, R., Bohn, T., Avis, C.A., Beerling, D.J., Chen, G., Eliseev, A.V., Denisov, S.N., Hopcroft, P.O., Lettenmaier, D.P., Riley, W.J., Singarayer, J.S., Subin, Z.M., Tian, H., Zürcher, S., Brovkin, V., van Bodegom, P.M., Kleinen, T., Yu, Z.C., Kaplan, J.O., 2013. Present state of global wetland extent and wetland methane modelling: conclusions from a model inter-comparison project (WETCHIMP). Biogeosciences 10, 753–788.
Meng, L., Paudel, R., Hess, P.G.M., Mahowald, N.M., 2015. Seasonal and interannual variability in wetland methane emissions simulated by CLM4Me ' and CAM-chem and comparisons to observations of concentrations. Biogeosciences 12, 4029–4049.
Miller, B.D., Carter, K.R., Reed, S.C., Wood, T.E., Cavaleri, M.A., 2021. Only sun-lit leaves of the uppermost canopy exceed both air temperature and photosynthetic thermal optima in a wet tropical forest. Agric. For. Meteorol. 301, 108347.
Mitidieri, N., 2014. Reservas De Carbono y Composición Florística En Dos Parcelas De 0.5Ha En Bosques Pantanosos "aguajales" Cercanos a Las Comunidades Quistococha y San Jorge en Loreto, Perú. Universidad Nacional de la Amazonía Peruana.
Oleson, K., Lawrence, D., Bonan, G., Drewniak, B., Huang, M., Koven, C., Levis, S., Li, F., Riley, W., Subin, Z., 2013. Technical Description of Version 4.5 of the Community Land Model (CLM). NCAR. National Center for Atmospheric Research (NCAR, Boulder, Colorado.
Oliveira, R.S., Eller, C.B., Barros, F.d.V., Hirota, M., Brum, M., Bittencourt, P., 2021. Linking plant hydraulics and the fast–slow continuum to understand resilience to drought in tropical ecosystems. New Phytol. 230, 904–923.
Pangala, S.R., Enrich-Prast, A., Basso, L.S., Peixoto, R.B., Bastviken, D., Hornibrook, E.R. C., Gatti, L.V., Marotta, H., Calazans, L.S.B., Sakuragui, C.M., Bastos, W.R., Malm, O., Gloor, E., Miller, J.B., Gauci, V., 2017. Large emissions from floodplain trees close the Amazon methane budget. Nature 552, 230–234.
Parolin, P., ARMBRüSTER, N., Junk, W.J., 2002. Seasonal changes of leaf nitrogen content in trees of Amazonian floodplains. Acta Amazon 32, 231. -231.
Paudel, R., Mahowald, N.M., Hess, P.G.M., Meng, L., Riley, W.J., 2016. Attribution of changes in global wetland methane emissions from pre-industrial to present using CLM4.5-BGC. Environ. Res. Lett. 11.
Putkinen, A., Siljanen, H.M., Laihonen, A., Paasisalo, I., Porkka, K., Tiirola, M., Haikarainen, I., Tenhovirta, S., Pihlatie, M., 2021. New insight to the role of microbes in the methane exchange in trees: evidence from metagenomic sequencing. New Phytol. 231, 524–536.
Renninger, H.J., Phillips, N., 2011. Hydraulic properties of fronds from palms of varying height and habitat. Oecologia 167, 925–935.
Restrepo-Coupe, N., Albert, L.P., Longo, M., Baker, I., Levine, N.M., Mercado, L.M., da Araujo, A.C., Christoffersen, B.O.D., Costa, M.H., Fitzjarrald, D.R., Galbraith, D., Imbuzeiro, H., Malhi, Y., von Randow, C., Zeng, X., Moorcroft, P., Saleska, S.R., 2021. Understanding water and energy fluxes in the Amazonia: lessons from an observation-model intercomparison. Glob. Chang. Biol. 27, 1802–1819.
Rey-Sánchez, A.C., Slot, M., Posada, J.M., Kitajima, K., 2016. Spatial and seasonal variation in leaf temperature within the canopy of a tropical forest. Clim. Res. 71, 75–89.
Ribeiro, K., Pacheco, F.S., Ferreira, J.W., de Sousa-Neto, E.R., Hastie, A., Krieger, G.C., Alvala, P.C., Forti, M.C., Ometto, J.P., 2021. Tropical peatlands and their contribution to the global carbon cycle and climate change. Glob. Chang. Biol. 27, 489–505.
Ricciuto, D., Sargsyan, K., Thornton, P., 2018. The Impact of Parametric Uncertainties on Biogeochemistry in the E3SM Land Model. J. Adv. Model. Earth Syst. 10, 297–319.
Ricciuto, D.M., Xu, X., Shi, X., Wang, Y., Song, X., Schadt, C.W., Griffiths, N.A., Mao, J., Warren, J.M., Thornton, P.E., 2021. An integrative model for soil biogeochemistry and methane processes: I. Model structure and sensitivity analysis. J. Geophys. Res. 126, e2019JG005468.
Riley, W.J., Subin, Z.M., Lawrence, D.M., Swenson, S.C., Torn, M.S., Meng, L., Mahowald, N.M., Hess, P., 2011. Barriers to predicting changes in global terrestrial methane fluxes: analyses using CLM4Me, a methane biogeochemistry model integrated in CESM. Biogeosciences 8, 1925–1953.
Roucoux, K.H., Lawson, I.T., Jones, T.D., Baker, T.R., Coronado, E.H., Gosling, W.D., Lähteenoja, O., 2013. Vegetation development in an Amazonian peatland. Palaeogeogr. Palaeoclimatol. Palaeoecol. 374, 242–255.
Safta, C., Ricciuto, D.M., Sargsyan, K., Debusschere, B., Najm, H.N., Williams, M., Thornton, P.E., 2015. Global sensitivity analysis, probabilistic calibration, and predictive assessment for the data assimilation linked ecosystem carbon model. Geosci. Model. Dev. 8, 1899–1918.
Saleska, S.R., Wu, J., Guan, K., Araujo, A.C., Huete, A., Nobre, A.D., Restrepo-Coupe, N., 2016. Dry-season greening of Amazon forests. Nature 531, E4–E5.
Sargsyan, K., Safta, C., Najm, H.N., Debusschere, B.J., Ricciuto, D., Thornton, P., 2014. Dimensionality reduction for complex models via Bayesian compressive sensing. Int. J. Uncertain. Quantif. 4.
Shi, X., Thornton, P.E., Ricciuto, D.M., Hanson, P.J., Mao, J., Sebestyen, S.D., Griffiths, N. A., Bisht, G., 2015. Representing northern peatland microtopography and hydrology within the Community Land Model. Biogeosciences 12, 6463–6477.
Shi, X.Y., Ricciuto, D.M., Thornton, P.E., Xu, X.F., Yuan, F.M., Norby, R.J., Walker, A.P., Warren, J.M., Mao, J.F., Hanson, P.J., Meng, L., Weston, D., Griffiths, N.A., 2021. Extending a land-surface model with Sphagnum moss to simulate responses of a northern temperate bog to whole ecosystem warming and elevated CO_2. Biogeosciences 18, 467–486.
Song, J., Miller, G.R., Cahill, A.T., Aparecido, L.M.T., Moore, G.W., 2021. Modeling profiles of micrometeorological variables in a tropical premontane rainforest using multi-layered CLM (CLM-ml). J. Adv. Model. Earth Syst. 13, e2020MS002259.
Tan, Z., Zeng, J., Zhang, Y., Slot, M., Gamo, M., Hirano, T., Kosugi, Y., Da Rocha, H.R., Saleska, S.R., Goulden, M.L., 2017. Optimum air temperature for tropical forest photosynthesis: mechanisms involved and implications for climate warming. Environ. Res. Lett. 12, 054022.
Teh, Y.A., Murphy, W.A., Berrio, J.-.C., Boom, A., Page, S.E., 2017. Seasonal variability in methane and nitrous oxide fluxes from tropical peatlands in the western Amazon basin. Biogeosciences 14, 3669–3683.
Thornton, P.E., Rosenbloom, N.A., 2005. Ecosystem model spin-up: estimating steady state conditions in a coupled terrestrial carbon and nitrogen cycle model. Ecol. Modell. 189, 25–48.
van Genuchten, M.T., 1980. A closed-form equation for predicting the hydraulic conductivity of unsaturated soils. Soil Sci. Soc. Am. J. 44, 892–898.
van Haren, J., Brewer, P.E., Kurtzberg, L., Wehr, R.N., Springer, V.L., Espinoza, R.T., Ruiz, J.S., Cadillo-Quiroz, H., 2021. A versatile gas flux chamber reveals high tree stem CH_4 emissions in Amazonian peatland. Agric. For. Meteorol. 307, 108504.
van Lent, J., Hergoualc'h, K., Verchot, L., Oenema, O., van Groenigen, J.W., 2019. Greenhouse gas emissions along a peat swamp forest degradation gradient in the Peruvian Amazon: soil moisture and palm roots effects. Mitigation and Adaptation Strategies for. Glob. Change 24, 625–643.
Werth, D., Avissar, R., 2004. The regional evapotranspiration of the Amazon. J. Hydrometeorol. 5, 100–109.
Wu, J., Albert, L.P., Lopes, A.P., Restrepo-Coupe, N., Hayek, M., Wiedemann, K.T., Guan, K., Stark, S.C., Christoffersen, B., Prohaska, N., 2016. Leaf development and demography explain photosynthetic seasonality in Amazon evergreen forests. Science 351, 972–976.
Wu, J., Serbin, S.P., Ely, K.S., Wolfe, B.T., Dickman, L.T., Grossiord, C., Michaletz, S.T., Collins, A.D., Detto, M., McDowell, N.G., 2020. The response of stomatal conductance to seasonal drought in tropical forests. Glob. Chang. Biol. 26, 823–839.
Xu, X., Elias, D.A., Graham, D.E., Phelps, T.J., Carroll, S.L., Wullschleger, S.D., Thornton, P.E., 2015. A microbial functional group-based module for simulating methane production and consumption: application to an incubated permafrost soil. J. Geophys. Res. 120, 1315–1333.
Xu, X., Yuan, F., Hanson, P.J., Wullschleger, S.D., Thornton, P.E., Riley, W.J., Song, X., Graham, D.E., Song, C., Tian, H., 2016. Reviews and syntheses: four decades of modeling methane cycling in terrestrial ecosystems. Biogeosciences 13, 3735–3755.

Yuan, F., Wang, Y., Ricciuto, D.M., Shi, X., Yuan, F., Brehme, T., Bridgham, S., Keller, J., Warren, J.M., Griffiths, N.A., 2021a. Hydrological feedbacks on peatland CH_4 emission under warming and elevated CO_2: a modeling study. J. Hydrol. (Amst.) 603, 127137.

Yuan, F., Wang, Y., Ricciuto, D.M., Shi, X., Yuan, F., Hanson, P.J., Bridgham, S., Keller, J., Thornton, P.E., Xu, X., 2021b. An integrative model for soil biogeochemistry and methane processes. II: warming and elevated CO_2 effects on peatland CH_4 emissions. J. Geophys. Res. 126, e2020JG005963.

Zhang, B., Tian, H., Lu, C., Chen, G., Pan, S., Anderson, C., Poulter, B., 2017. Methane emissions from global wetlands: an assessment of the uncertainty associated with various wetland extent data sets. Atmos. Environ. 165, 310–321.

Zhang, J., Griffis, T.J., Baker, J.M., 2006. Using continuous stable isotope measurements to partition net ecosystem CO_2 exchange. Plant Cell Environ. 29, 483–496.

Zhuang, Q., Melillo, J.M., Sarofim, M.C., Kicklighter, D.W., McGuire, A.D., Felzer, B.S., Sokolov, A., Prinn, R.G., Steudler, P.A., Hu, S., 2006. CO_2 and CH_4 exchanges between land ecosystems and the atmosphere in northern high latitudes over the 21st century. Geophys. Res. Lett. 33.